Determination of the Relationship between the Geometric Structure of a Model Peptide and Its ^{13}C Isotope-Edited FTIR Spectroscopy by ATR in H_2O

by

Olaa Eid Alharbi

A Thesis Submitted In Partial Fulfillment

of the Requirements for the Degree of

Master of Science in Chemistry

Middle Tennessee State University

December 2014

Thesis Committee:

Dr. Chengshan Wang, Major Professor

Dr. Jing Kong

Dr. Keying Ding

I dedicate this research work to my family

ACKNOWLEDGMENTS

I am using this opportunity to express my gratitude to everyone, who supported me throughout this thesis. I am thankful for their aspiring guidance, invariably constructive criticism, and friendly advice during the project work. I express my warm thanks to my advisor Dr. Chengshan Wang for the continuous support of my master study and research, for his patience, motivation, enthusiasm, and immense knowledge. His guidance helped me in all the time of research and writing of this thesis. I could not have imagined having a better advisor and mentor for my master study.

I would also like to thank my research committee Dr. Jing Kong and Dr. Keying Ding for reviewing my thesis and giving me valuable suggestions for my work, special thanks also for Dr. Leblanc of the university of Miami for ATR-FTIR and CD measurements. My sincere thanks also goes to my great husband (Naif Aljuaid) for his help and support all the time. Last but not least, I would greatly thank my parents, sisters and brothers for their love and their encouragement I would not have accomplished my goals without their support.

ABSTRACT

Determination of protein structures (such as α-helix, β-sheet, unstructured conformation, and so on) is important to correlate the function of a protein with its structure.[1] X-ray crystallography is a powerful technique but it requires proteins to form single crystal structure. However, lots of proteins do not meet this requirement. NMR can determine the structure of peptides/proteins in aqueous environment but the measurement is time-consuming. Thus, determination of the structure of proteins/peptides with short life-time (such as one hour) in aqueous solution is challenging for NMR. Recently, IR spectroscopy has been reported to be able to address the geometric structure of peptide with ^{13}C isotopic labels in deuterated water (D_2O) in residue level.[2] Although similar to regular water, D_2O is not physiologically approved.[3] On the other hand, H_2O has intensive absorption around 1620 cm^{-1} (this will cover the IR absorption of proteins/peptides) in IR spectroscopy. Thus, traditional transmission measurement of IR spectra of proteins/peptides in H_2O will fail, because the thickness of normal liquid FTIR cell is in millimeter level.

In this thesis, ^{13}C isotope edited FTIR was applied in H_2O solution by attenuated total reflection (ATR) technique, which can avoid H_2O background absorption because the path-length of IR in the sample solution of ATR is only several micrometers. A model helical peptide Ac-AAAAKAAAAKAAAAKAAAAY-NH_2 (Ac means C-terminus and NH_2 indicates the N-terminus) was synthesized and ^{13}C labeled alanine (A) residues were introduced into the model peptide with

various spacing residues. The ^{13}C labeled residues generate a new amide I band, namely, ^{13}C amide I band which was shown to relate to the geometry of the helical peptide. For example, the ^{13}C amide I band was detected at 1608 cm^{-1} when the two ^{13}C labeled A residues are adjacent. When the number of spacing residues increased to 2 and 3, the ^{13}C amide I band was detected at 1599 and 1602 cm^{-1}, respectively. Thus, the ^{13}C amide I band can help to determine the geometry of peptides/proteins.

TABLE OF CONTENTS

PAGE

LIST OF FIGURES

FIGURE **PAGE**

LIST OF TABLES

TABLE **PAGE**

LIST OF SCHEMES

SCHEME **PAGE**

CHAPTER I

INTRODUCTION

1.1 Structural Biology

Proteins are complex biological macromolecules, consisting of chains of amino acids covalently linked by amide bonds.[1-4] All proteins found in biological systems are composed of 20 different amino acids. As shown in Figure 1, amino acids consist of one amino group, one carboxylic acid group, and an α-carbon which links R groups which is also called the residue group. Amino acids are distinguished based on the structure of the R group (Table 1).

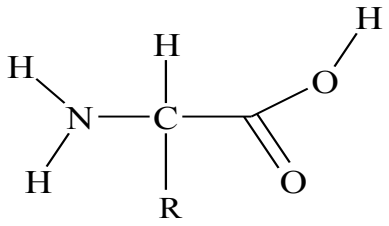

Figure 1: Structure of an amino acid

Table 1. Structure of R group of amino acids

Amino acid	**Abbrevations**		**Structure of R group**
Alanine	Ala	A	$-CH_3$
Arginine	Arg	R	$-(CH_2)_3-NH-C(NH_2)=NH$
Asparagine	Asn	N	$-CH_2-CO-NH_2$

Table 1 (Continued). Structure of R group of amino acids

Aspartic acid	Asp	D	$-CH_2-COOH$
Cysteine	Cys	C	$-CH_2-SH$
Glutamine	Gln	Q	$-(CH_2)_2-CO-NH_2$
Glutamic Acid	Glu	E	$-(CH_2)_2-COOH$
Glycine	GlY	G	-H
Histidine	His	H	$-CH_2C_3H_3N_2$
Isoleucine	Ile	I	$-CH(CH_3)-CH_2-CH_3$
Leucine	Leu	L	$-CH_2-CH-(CH_3)_2$
Lysine	Lys	K	$-(CH_2)_4NH_2$
Methionine	Met	M	$-(CH_2)_2-S-CH_3$
Phenylalanine	Phe	F	$-CH_2-C_6H_5$
Proline	Pro	P	$-CH(CH_2)_3NH$
Serine	Ser	S	$-CH_2-OH$
Threonine	Thr	T	$-CH(OH)-CH_3$
Tryptophan	Trp	W	$-CH_2-C_8H_6N$
Tyrosine	Tyr	Y	$-CH_2-C_6H_5-OH$
Valine	Val	V	$-CH-(CH_3)_2$

Proteins are essential to life processes. They perform a variety of functions, including catalyzing metabolic reactions,[5-9] replicating DNA,[10, 11] responding to stimuli,[12, 13] and so on. Malfunction of proteins has been shown to be related to many diseases.[5, 7, 8, 14-17] Therefore, the elucidation of proteins structure will not only help to understand how proteins work in vivo but also

provide pathological information about many diseases. As a consequence, structural biology which focuses on the elucidation of protein structure has attracted extensive scientific attentions.[18-21] For example, the determination of the structure of the photosynthesis center was awarded Nobel Prize for 1988[18] and the 2009 Nobel Prize was awarded to Venkatraman Ramakrishnan, Thomas A. Steitz, and Ada Yonath for the elucidation of the structure of ribosome.[8, 19, 20]

1.2 Protein Structure

1.2.1 Primary Structure

Amino acids are covalently linked together by an amide bond (i.e., CO-NH), formed between the amine group of one amino acid and the carboxyl group of the adjacent amino acid.[3] A chain of amino acids connected by amide bonds is referred to as a polypeptide chain. The two termini of a polypeptide chain are called N-terminus (it has free amine group) and C-terminus (it has free carboxylic acid group). The primary structure of a polypeptide is usually written from N-terminus to C-terminus. Figure 2 is an example of protein primary structure.

DAEFRHDSGYEVHHQKLVFFAEDVGSNKGAIIGLMVGGVVIA

Figure 2. Sequence of β-amyloid which is hallmark protein of Alzheimer's disease. Each letter represents one amino acid (*cf.* Table 1).

1.2.2 Secondary Structure

Secondary structure refers to the sequential arrangement of amino acids in a polypeptide chain and it is characterized by the intra and intermolecular hydrogen bonds among the amino acid residues. Typical secondary structures (also called as conformations) includes α-helix, β-sheets, and random coils.[22-24] The random coils structure is also called unstructured conformation. The polypeptide chain in this structure is well dissolved in the aqueous solution and moves freely in the aqueous environment.[24] The residues in the polypeptide chain do not substantially form hydrogen bonds substantially with each other, but form hydrogen bonds with H_2O molecules in solution.

As the most common secondary structure, the α-helix looks like a spring as shown in Figure 3. α-Helix is characterized by the intra-molecular hydrogen bonds between the amino group of one amino acid and the carbonyl group of another amino acid located 3~4 residues away along the polypeptide chain (*cf.* Figure 3).[23] These hydrogen bonds are usually present parallel to the helical axis. The α-helix is usually right handed and contains approximately 3.6 amino acid residues per turn. Formation of hydrogen bonds creates helical structure of the polypeptide chain. Side chains of amino acids in α-helix protrude out of the helix.

The structural units of β-sheets are strands, which is a fully extended structure characterized by multiple strands (polypeptide chains) arranged side-by-side as shown in Figure 3.[22] Each β-sheet contains 6 to 22 strands. Residue groups are present above or below the plane of polypeptide chain. Inter-strand hydrogen bonds are formed between the carbonyl oxygen of one chain and the

amide hydrogen of another chain. β-sheet includes two types, namely, parallel and anti-parallel sheets. In a parallel sheet, two strands run in the same direction (shown in Figure 3). In an anti-parallel sheet, the neighboring strands run in opposite direction. For example, if one strand runs from N- terminus to C-terminus, the neighboring strand runs from C-terminus- N-terminus.

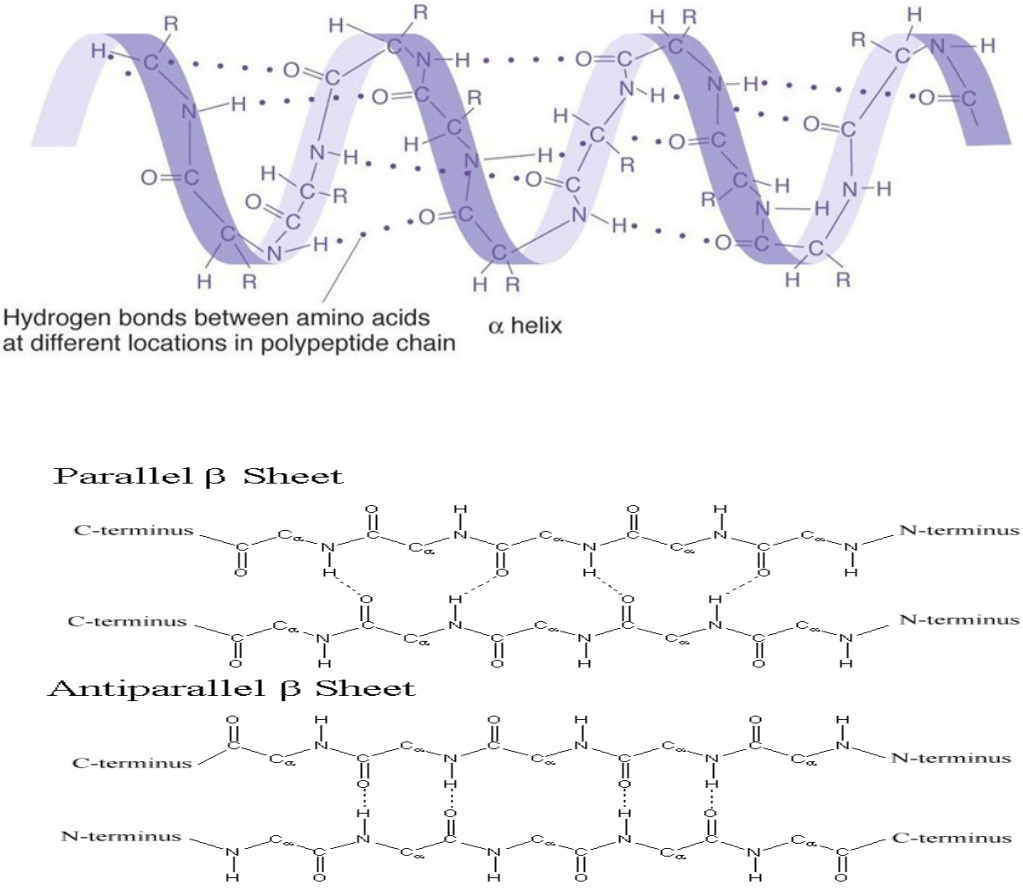

Figure 3: Illustration of secondary structures.

1.2.3 Tertiary Structure

Tertiary structure arises when secondary structure elements pack tightly to form a well-defined 3D structure.[25, 26] It is usually stabilized by four forces, hydrophobic forces, covalent bonds, Vanderwall interactions, and hydrogen bonds. Among these four forces, hydrophobic interactions among the secondary structural elements play an important role in stabilizing the tertiary structure. Tertiary structure is also called the native state of the protein. It is possible for two residues that are far away in the sequence (or the primary structure) to be adjacent to each other in the tertiary structure. To determine proteins structure (i.e, primary, secondary, and tertiary structure), various techniques have been developed. Some of the most important techniques are discussed below.

1.3 Techniques to Determine Protein Structure

1.3.1 X-ray Crystallography

X-ray crystallography is the most widely used method to address protein structure and the detailed proteins structure can be determined in atomic level.[27, 28] Most of the protein structures in Protein Data Bank were determined by this method.[1] However, this technique has some drawbacks. First, proteins should form single crystal structure for X-ray measurement and there is no particular common crystallization method that can be applied to all proteins. It is difficult for many proteins to form single crystal structure. For example, β-amyloid protein (Aβ) which contains 40-42 amino acids is the hallmark protein of Alzheimer's disease (*cf.* Figure 2). Effort has been made to crystallize Aβ for more than 20

years. However, formation of the single crystal structure of Aβ has not been reported. Second, although they are able to affect the structure of proteins, artificial solvents are usually needed to facilitate the crystallization of proteins. In addition, the movement of protein is reduced in a crystal state. This creates a static environment, which may be different from the dynamic aqueous environment in which proteins reside in biological systems.

1.3.2 NMR Spectroscopy

Another powerful technique is multi-dimensional NMR. The major advantage of NMR spectroscopy is that it can determine protein structure in aqueous environment, which is favorable for proteins.[29-33] However, various amounts of deuterated water, also called heavy water (D_2O) which is not solvent in biological systems, needs to be added into the solution to lock the magnetic field of NMR. Furthermore, measurement of the NMR spectra of proteins is time intensive and the interpretation is complicated.[29-33] This makes it impossible for NMR to determine the protein structural elements which have a short lifetime.[33] As mentioned above, it has been reported that the small aggregates (i.e., oligomers) of Aβ are toxic to neuronal cells in the brain and the oligomer's lifetime can last one or several hours.[33] Therefore, faster methods to determine proteins structure have been developed. The two mostly widely used techniques are circular dichroism (CD) and IR spectroscopy.

1.3.3 Circular Dichroism (CD) Spectroscopy

There is a long history of CD studies about the structure of peptides/proteins in the biochemical and biophysical sciences.[24, 34-39] CD is very sensitive to protein conformation and is a fast method for monitoring structural changes, because the measurement of CD can be accomplished in minutes or even seconds. Due to the large amount of carbonyls (C=O which have intense absorption around 200 nm) in the amide bonds, proteins usually show strong CD signals between 260 and 180 nm.[24, 38, 39] Since the carbonyls are arranged differently in conformations (such as α-helix, β-sheets, and unstructured conformation), every secondary structure shows its distinct patterns in CD spectrum as below.[34, 37]

The Far-UV CD spectra of the α-helix conformation have two characteristically negative peaks at 222 and 208 nm and one positive peak at 192 nm. The Far-UV CD spectrum of β-sheet conformation exhibits a positive peak at 196 nm and a negative peak at 215 nm. As for the unstructured conformation, only one negative peak at 199 nm will be detected (Figure 4).[34, 37] Similarly, every conformation can also show its distinct pattern in FTIR spectroscopy.

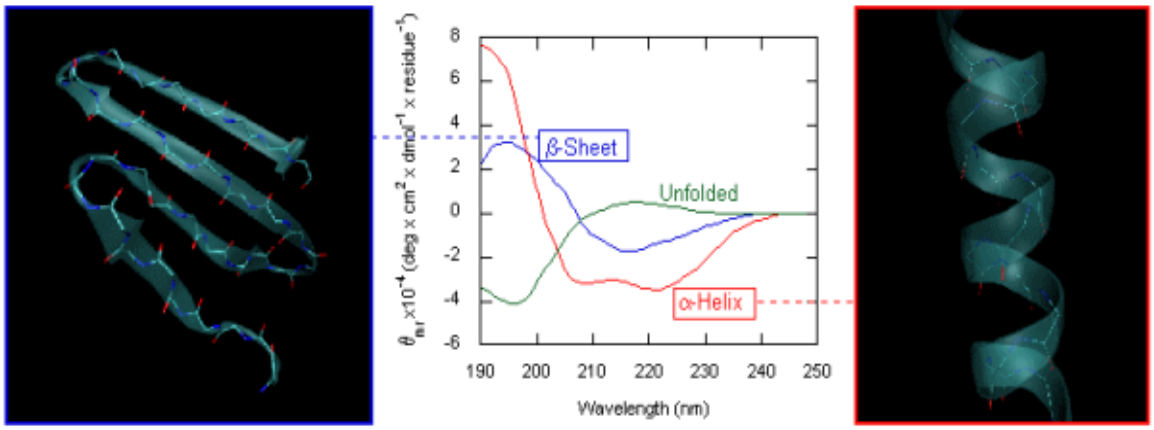

Figure 4**:** The secondary structure conformation and the CD spectra of protein structural elements. Right is an example of the backbone conformation of a peptide in α-helix and left is in β-sheet. The center is the CD spectra of different conformations.

1.3.4 FTIR Spectroscopy

Infra-red (IR) spectroscopy is another widely used technique for the analysis of secondary structure of peptides.[24, 38-47] The advantage of IR spectroscopy over other techniques is that it can be applied to wide range of sampling conditions like powders, crystals, solid dosage forms, crystals. Furthermore, the amount of sample required for analysis is very small. Even membrane proteins can be analyzed by this method.[24, 38, 39, 43, 46, 47] After the development of Fourier Transform Infra-Red (FTIR) spectrometers, spectra of high accuracy were obtained and instrument S/N ratio was also improved. In addition, FTIR spectrum can be obtained in several seconds to several minutes, depending on the number of scans taken. Thus, FTIR spectroscopy became a

powerful tool in conformational analysis of proteins/peptides, especially for the detection of transitional conformation change during local environmental changes such as temperature or pH.

In FTIR spectroscopy, peptides/proteins absorb the infrared radiation and give rise to nine characteristic bands namely Amide A, B, and I-VII.[24, 38, 39, 43, 46] Frequencies and description of these amide bands are shown in Table 2. Among all these bands, Amide I and Amide II bands are found to be most prominent bands in the spectra of proteins. Amide I band is found around 1600-1700cm $^{-1}$ and it is mainly associated with C=O stretching vibrations (over 85 %). Amide II band derives mainly from N-H bending vibrations (40-60%) as well as C-N stretching vibrations (18-40%), and this band is found to be less sensitive to the conformation of proteins when compared to amide I band. All the other bands are found to result from the overlapping of different vibrations. Consequently, they are less useful in protein conformational studies.

Table 2. Characteristics infrared bands of peptide linkage

Designation	Approximate Frequency (cm^{-1})	Description
Amide A	3300	NH stretching
Amide B	3100	NH stretching
Amide I	1600-1690	C-O stretching
Amide II	1480-1575	CN stretching, NH bending
Amide III	1229-1301	CN stretching, NH bending
Amide IV	625-767	OCN bending
Amide V	640-800	Out-of-plane, NH bending

Table 2 (Continued). Characteristics infrared bands of peptide linkage

Amide VI	537-606	Out-of-plane, C-O bending
Amide VII	200	Skeletal torsion

In the Amide I region (1600-1700cm^{-1}), each type of secondary structure (α-helix, β-sheet, or unstructured conformation) gives rise to a unique frequency due to the different hydrogen bonding pattern among them.[38, 39, 46] The IR absorption frequencies of different types of secondary structures are shown in Table 3. For example, unstructured conformation shows a peak at ~1640 cm^{-1} for the amide I band and the peak of β-sheet is ~1630 cm^{-1}. As for α-helix, the peak position is somewhat complicated because the position is affected by the length of the helix. For a long helix, the peak will appear at ~1648 cm^{-1} and moves to higher frequency when the helix becomes shorter.

Table 3. Characteristic amide I frequencies of Protein secondary structure

Frequency(cm^{-1})	Assignment
1690-1680	β-sheet structure
1657-1648	helix
1645-1640	Random coil
1630-1620	β-sheet structure

1.3.5 Quantitative Estimation of Secondary Structures in Certain Protein

As mentioned in section 1.3.1 and 1.3.2, x-ray crystallography can provide structural information in atomic level but required target proteins to form single crystal. Multi-dimensional NMR can analyze the proteins structure in solution with high resolution, but the measurement is quite time-consuming. Therefore, quantitative estimation of secondary structure of protein has been tried by CD and FTIR. The basic assumption of the quantitative estimation of secondary structure of protein is that proteins/peptides are a linear sum of a few fundamental secondary structural elements and the percentage of each element is only related to spectral intensities.

As for CD spectroscopy, softwares (such as CONTIN, CDSSTR, SELCOM, and CD-Pro) have been developed to calculate the percentage of every secondary structural element in proteins by CD spectroscopy.[35, 37-39, 48] For example, Dr. Chengshan Wang *et al* have shown that the CD spectra of aequorin (a bio-fluorescence protein) are affected by pH. The negative peaks at 208 and 222 nm reach the maximum at pH 7.6, because increasing or decreasing the pH values will decrease the peaks intensity. This indicates that aequorin contains the highest percentage of α-helix at pH 7.6. To get more detailed information, the CD spectra were analyzed by CD-Pro and the results are shown in Table 4. When the pH increases, the percentage of α-helix decreases and that of unstructured conformation increases. Thus, the increase of pH change some α-helix in aequorin to unstructured conformation. When pH decreases, the percentage of

β-sheet increases, which indicates the transformation of some some α-helix in aequorin to β-sheet.[38]

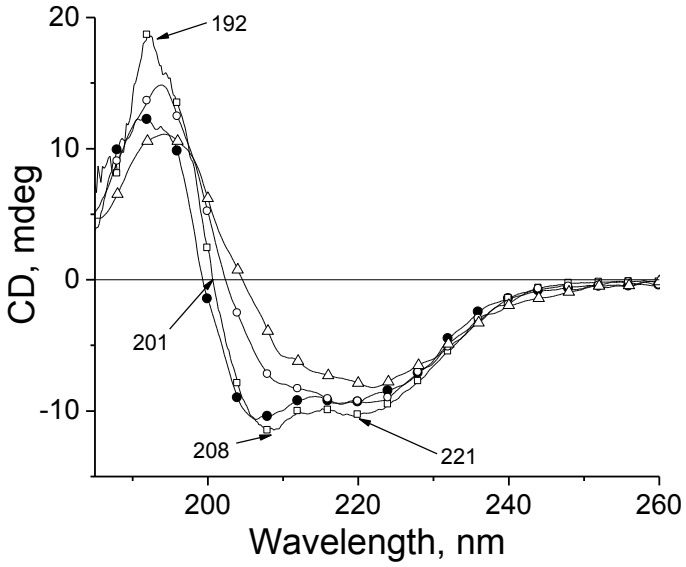

Figure 5: Circular dichroism spectra of aequorin at concentration of 0.1 mg·ml^{-1} under different pH values: -●- 9.0, -□- 7.6, -○- 4.8, -Δ- 4.0.

Table 4. Content in percentage of secondary structures of aequorin in aqueous solution under different pH conditions.

pH	α-helix	β-sheet	Unstructured
9.0	32.2 %	14.8 %	53.1 %
7.6	37.8 %	13.5 %	48.9 %
4.8	30.9 %	20.1 %	49.3 %
4.0	23.9 %	27.8 %	47.5 %

Similarly, curve fitting procedure can be applied to FTIR spectra, which can resolve convolutions of absorption bands. The percentage of secondary structures can be quantitatively estimated after the resolution enhancement of amide I spectra by FSD technique. Dong *et al.* reported the distribution of secondary structures determined from the amide I spectra of globular proteins, which was nearly identical to the amount computed from crystallographic data.[49]

Although overall content of secondary structures in proteins/ peptides can be investigated by IR and CD spectroscopy, structural elements (α-helix, β-sheets) cannot be assigned to specific amino acid residues in polypeptide sequence. Therefore, a new technique called ^{13}C isotope-edited FTIR spectroscopy has been used to improve the low resolution results of traditional CD or FTIR to “medium resolution”.

1.3.6 ^{13}C Isotope-edited FTIR Spectroscopy

^{13}C isotope-edited FTIR spectroscopy has been reported in 1991[50-53] and used for several proteins/peptides to probe the structures of particular regions within a protein, elucidate the protein-protein and protein-peptide interactions, and determine orientation of peptides and proteins in phospholipid membranes.[50-53] Later, it was applied to study the synthesized model peptides and was reported to address the secondary structure information in residue level in deuterated water.[54-57] This job cannot be accomplished by either traditional IR or CD spectroscopy. The proof-of-principle test of ^{13}C isotope-edited IR

spectroscopy was accomplished on a model peptide with mixture conformation of α-helix and unstructured conformation. The details of this technique are presented below.[56]

The peptide with sequence Ac-YAAKAAAKAAAAKAAH-NH_2 (Ac means C-terminus and NH_2 indicates the N-terminus) has been shown to have a mixture of unstructured conformation and α-helix in D_2O.[56] Dr. Decatur and coauthors have synthesized four double ^{13}C labeled peptides Ac-YAAKAAAKAAAAKAAH-NH_2 (referred as Pep17 shown in Scheme 1) by using ^{13}C labels to replace the regular carbons in the sequence, starting from C-terminus to N-terminus. The FTIR spectra of all of the peptides were obtained in D_2O from 0 to 45°C.

Ac-Y<u>AA</u>KAAAKAAAAKAAH-NH_2 (17L1)

Ac-YAAKA<u>AA</u>AKAAAAKAAH-NH_2 (17L2)

Ac-YAAKAAAAKA<u>AA</u>AKAAH-NH_2 (17L3)

Ac-YAAKAAAAKAAAAK<u>AA</u>H-NH_2 (17L4)

Scheme 1: Sequence of the ^{13}C double labeled peptides. The carbonyls of underlined residues are replaced by ^{13}C labels.

When the temperature increases to 45 °C, CD results showed that almost all of the residues in the peptide are in unstructured conformation.[56] ^{13}C labels in the peptide do not change this property and the amide I band of the ^{13}C labeled carbonyls (^{13}C=O) in unstructured conformation is identical to that of regular

amide I band (at 1640 cm^{-1} in D_2O), because carbonyls interact with solvent molecules very well. When the ^{13}C labeled residue is in α-helix, the amide I band of ^{13}C labeled residue (referred as ^{13}C amide I band in the following) moves to 1602 cm^{-1}, which is different to the regular amide I band of α-helix at 1630 cm^{-1} in D_2O.

When the temperature decreases to 0 °C, CD results showed that lots of residues in the peptide transform to α-helix but several residues remain in the unstructured conformation. Which residues still remain in the unstructured conformation? To address this question, the FTIR spectra of 17L1 to 17L4 in D_2O were measured and the results are shown in Figure 6. As for the unlabeled peptide, no ^{13}C amide I band was detected. For 17L2, 17L3, and 17L4, the ^{13}C amide I band was detected at 1602 cm^{-1}, which means that residues 2, 3, 6, 7, 11, and 12 transform to α-helix at 0 °C. However, the ^{13}C amide I band does not appear in 17L4 even at 0 °C. This indicates that residues 15 and 16, which are ^{13}C labeled in 17L4, are still in unstructured conformation at 0 °C. By the presence or absence of ^{13}C amide I band in the FTIR spectrum of selectively ^{13}C labeled peptide, the conformation of every residue can be determined by the ^{13}C isotope-edited FTIR spectroscopy.

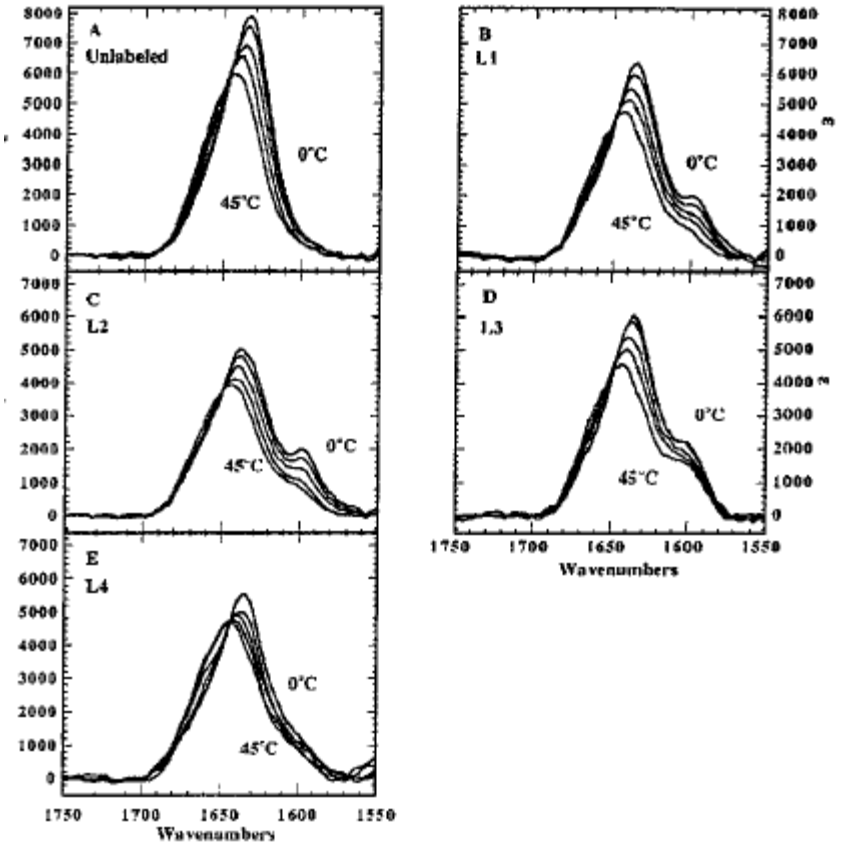

Figure 6: FTIR spectra of unlabeled (A) and labeled (B for 17L1, C for 17L2, D for 17L3, and E for 17L4) at 0, 15, 25, and 45 °C.

1.3.7 Applications of ^{13}C Isotope-edited FTIR Spectroscopy to Obtain Geometric information about the Structure of α-helix

More detailed information can be obtained by ^{13}C isotope-edited FTIR spectroscopy. As mentioned above, the regular amide I band of α-helix appears at 1630 cm^{-1} in D_2O when both the neighboring carbonyls are regular $^{12}C=O$ (Scheme 2A). The ^{13}C labeled residue has been reported to decrease the ^{13}C amide I band to ~1600 cm^{-1} and the ^{13}C amide I band position is related to the geometry of the helix. When the two ^{13}C labeled residues are adjacent (Scheme

2B), the ^{13}C amide I band is at 1600 cm^{-1}. If there are spacing regular residues between the two ^{13}C labeled residues which are close to each other in the helix (Scheme 2C), a strong coupling between ^{13}C=O (i.e. ^{13}C-^{13}C coupling) occurs and the ^{13}C amide I band will further decrease to 1592 cm^{-1}, which can be used as a fingerprint peak to determine the geometry in α-helix.[54, 55, 58] If all the neighboring residues have been determined, the structure of α-helix model peptide will be determined as a consequence.[54, 58]

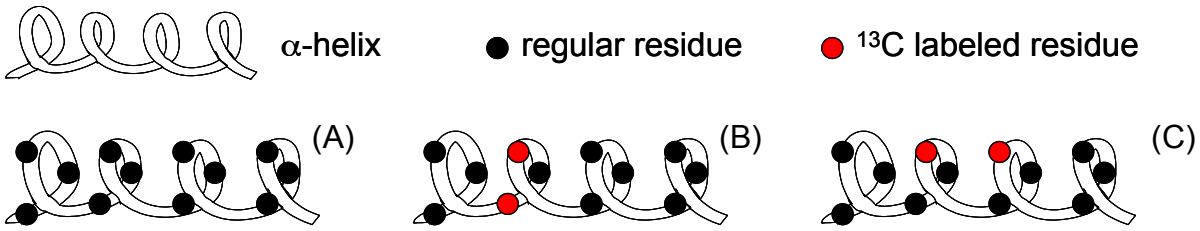

Scheme 2: Hydrogen bond formation between the amide groups in α-helix. The atoms in red are ^{13}C labeled residues.

For example, double ^{13}C labels have been introduced into the sequence of Pep25 as shown in Scheme 3. There are 0, 1, 2, and 3 spacing regular residues between the double ^{13}C labeled residues in L1, L2, L3, and L4, respectively. As for L1, both amide I band at 1630 cm^{-1} and ^{13}C amide I band at 1600 cm^{-1} were detected.[54, 58] This indicates that residues 12 and 13 are not neighboring residues in the α-helix. The same results were obtained in the FTIR spectra of L2 and L4. Thus, neither residues 11&13 nor residues 9&13 are neighboring residues in the α-helix, since the ^{13}C amide I band of ^{12}C-^{13}C coupling was

detected. However, the ^{13}C amide I band of the FTIR spectrum of L3 was determined to be 1590 cm^{-1}. Therefore, residues 11 and 14, which are ^{13}C labeled in 25L-3, are close to each other in the α-helix as shown in Scheme 2C.

Ac-AAAAKAAAKAAAKAAAAKAAAAKAAAAY-NH_2 (L1)

Ac-AAAAKAAAKAAAKAAAAKAAAAKAAAAY-NH_2 (L2)

Ac-AAAAKAAAKAAAAKAAAAKAAAAKAAAAY-NH_2 (L3)

Ac-AAAAKAAAKAAAAKAAAAKAAAAKAAAAY-NH_2 (L4)

Scheme 3: Sequence of the ^{13}C double labeled pep25. The carbonyls of underlined residues are replaced by ^{13}C labels.

1.3.8 Challenge of ^{13}C Isotope-edited FTIR Spectroscopy

It is worth noting that all of the ^{13}C isotope-edited FTIR spectroscopy was performed in D_2O, not H_2O. Although D_2O and water are quite similar, their physiological properties are quite different.[59-61] Proteins can exhibit their function only in normal water.[59, 62] In addition, D_2O is also expensive and harmful to health.[59] Therefore, further application of ^{13}C isotope-edited FTIR spectroscopy of proteins/peptides in H_2O is important. However, since H_2O has an intense absorption band around 1610 cm^{-1} (shown in Figure 7)[63] which will cover all the peaks of α-helix and β-sheet, direct measurement of FTIR spectra of peptides/proteins in H_2O solution by traditional cells will fail.

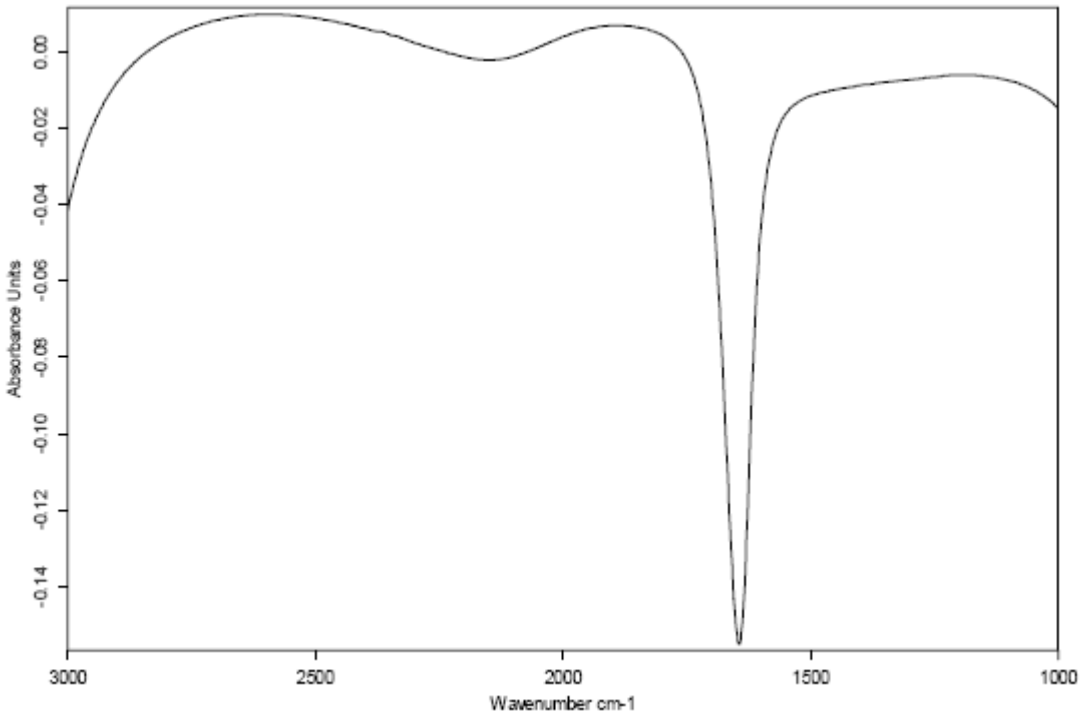

Figure 7: Intensive IR absorption of H_2O around 1610 cm^{-1}.

1.3.9 ATR Technique can Help to Avoid H_2O Background Absorption

Recently, attenuated total reflection (ATR) technique has been developed to determine the IR spectroscopy of proteins/peptides in H_2O solution.[38, 39, 64-69] Different to traditional liquid IR cells with path length on the orders of millimeters, the path-length of IR radiations through the sample solution of ATR is only several micrometers, because the ATR crystal reflects the incident IR beam which goes into the interface of sample by several micrometers (shown in Figure 8).

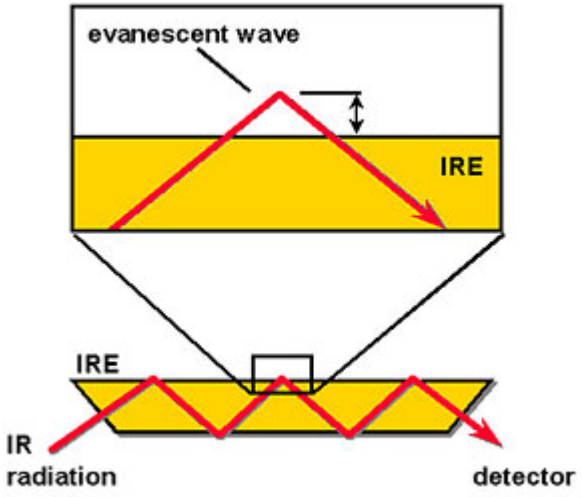

Figure 8: Illustrations of the ATR technique.

In addition, we have just shown that ATR technique can avoid the H_2O background absorption and can help the application of ^{13}C isotope-edited IR spectroscopy in H_2O as following. First, the unlabeled Pep17 was dissolved in H_2O at pH 5.0 and 12.5. The conformation of Pep17 in H_2O solution at the two pH values was evaluated by CD spectroscopy and the results are shown in Figure 9. As for pH 12.5, two negative peaks were detected at 208 and 222 nm, which are the charateristic peaks of α-helix. When pH decreased to 5.0, only one negative peak (shown in the inset of Figure 9) was detected at 198 nm, which was asssigned to unstructured conformation. The CD results show that the majority of Pep17 is in α-helix at pH 12.5 and changes to unstructured conformation at pH 5.0. The ^{13}C labeled Pep17 showed the identical results to those of unlabled Pep17. To determine the conformation of specific residues,

Pep17 peptides in H_2O solutions at pH 5.0 and 12.5 were examined by ATR-FTIR spectroscopy.

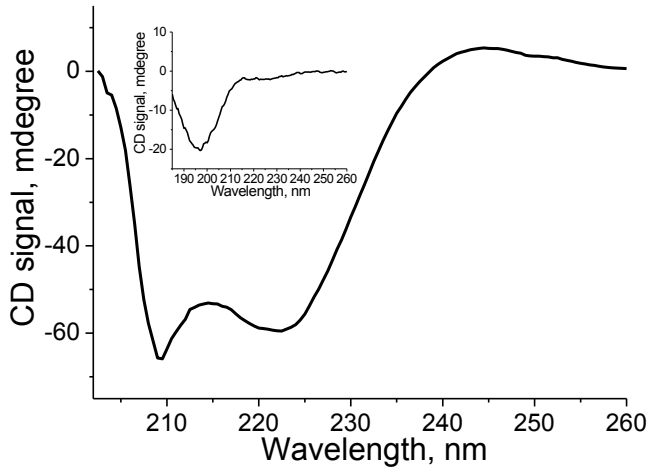

Figure 9: CD spectra of unlabeled Pep17 at pH 12.5 and 5.0 (inset) with a concentration of 0.44 and 0.10 mg/ml, respectively.

Figure 10 shows the ATR-FTIR spectra of unlabeled Pep17 and 17L2 (^{13}C labeled at residues 6&7) at pH 5.0. Both of these peptides showed an amide I band at 1640 cm^{-1}, which is the characteristic peak of unstructured conformation. Therefore, ATR-FTIR results correlate to the CD results very well. Amide II band was also detected at 1545 cm^{-1}, which is typical for peptides/proteins in H_2O solution. Little difference was detected between the ATR-FTIR spectra of unlabeled Pep17 and 17L2. In addition, the ATR-FTIR spectra of 17L1, 17L3, and 17L4 are identical to that of 17L2. Therefore, in H_2O solution, the ^{13}C amide I band is similar to regular (i.e., ^{12}C) amide I band when the residue is in

unstructured conformation. This is similar to the FTIR spectra of Pep17 in D_2O solution.[56]

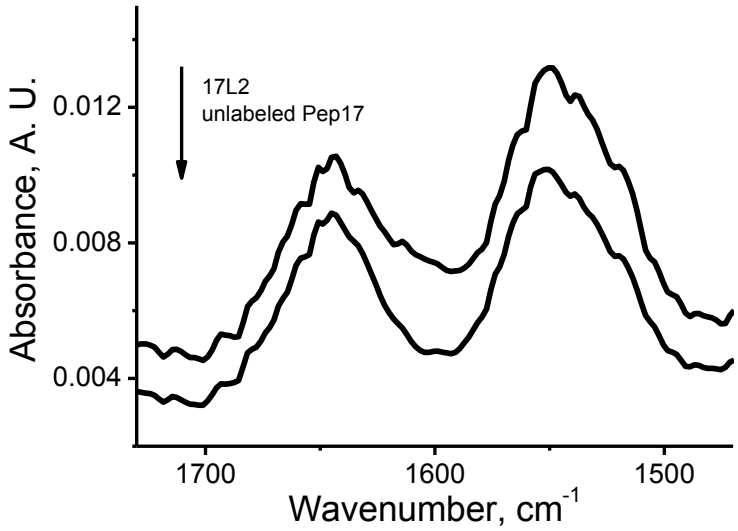

Figure 10: ATR FTIR spectra of unlabeled Pep17 and 17L2 in H_2O at pH 5.0.

When pH increased to 12.5, both amide I and amide II bands were detected in the ATR-FTIR spectrum of unlabeled Pep17 as shown in Figure 11. The broad amide I band from 1620 to 1640 cm^{-1} may comprise three components. The amide I band of α-helix of Pep17 was at 1630 cm^{-1} in D_2O. It has been reported that the amide I band of α-helix in H_2O will be ~6 cm^{-1} higher than that in D_2O.[24] Thus, the first component of the broad amide I band of unlabeled Pep17 is the amide I band from α-helix. Second, the deformation peak of H_2O in NaOH may cause the peak around 1620 cm^{-1}.[70] Third, some residues of Pep17 may be still in unstructured conformation even at pH 12.5. The amide I

band of the unstructured part of Pep17 will be at 1640 cm^{-1}. To determine the residues in unstructured conformation at pH 12.5, ATR-FTIR spectra of ^{13}C labeled Pep17 were also measured as shown in Figure 11.

As for 17L4 (cf. Figure 11), not only the broad amide I band but also a shoulder peak at 1602 cm^{-1} were detected in the ATR-FTIR spectrum. Since the only difference between unlabeled Pep17 and 17L4 is the presence of ^{13}C labeled carbonyls in 17L4, the peak at 1602 cm^{-1} is the ^{13}C amide I band. Notice that the ^{13}C amide I band of α-helical Pep17 in D_2O was detected at 1596 cm^{-1}. It is reasonable that the ^{13}C amide I band of α-helical Pep17 in H_2O is 6 cm^{-1} higher. As mentioned above, Figure 10 shows that no ^{13}C amide I band should be detected if the ^{13}C labeled residues are in unstructured conformation. Thus, the presence of ^{13}C amide I band at 1602 cm^{-1} in the ATR-FTIR spectrum of 17L4 indicates that residues 15 and 16 are in α-helical conformation at pH 12.5. Similarly, ^{13}C amide I band was also clearly detected in the ATR-FTIR spectra of 17L2 and 17L3. Consequently, residues 6, 7, 11, and 12 are also in in α-helical conformation at pH 12.5. However, the ^{13}C amide I band was absent in the ATR-FTIR spectrum of 17L1. This suggests that residues 2 and 3 are still in unstructured conformation at pH 12.5. As a consequence, the conformation of specific residues in a peptide was shown here to be able to be screened by the ^{13}C amide I band around 1602 cm^{-1} as a “fingerprint” peak.

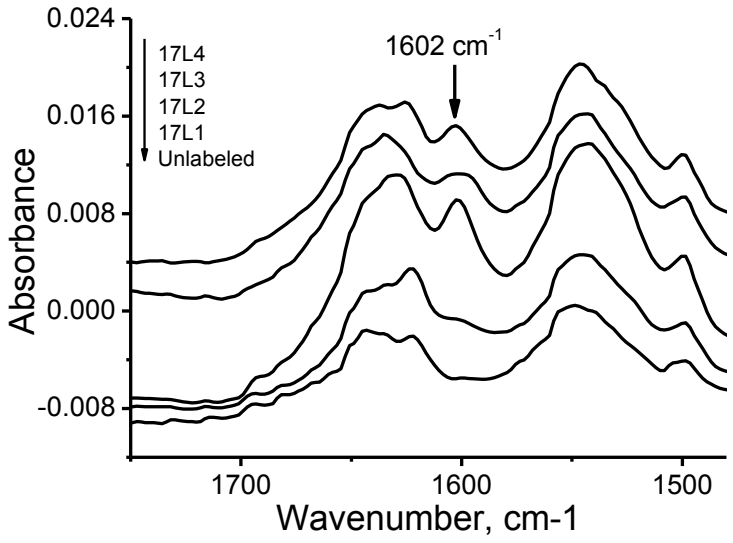

Figure 11: ATR FTIR spectra of unlabeled and ^{13}C labeled Pep17 at pH 12.5.

1.4 My Thesis Project

As mentioned in section 1.3.6 and 1.3.7, ^{13}C isotope-edited IR spectroscopy can not only determine the conformation of specific residues (cf., section 1.3.6) but also the geometric information about the structure of the helix (cf., 1.3.7). Although we have shown that ATR technique can help to avoid the intensive H_2O background absorption and determine the conformation of specific residues in H_2O, whether ATR can further help to provide geometric information has not been verified. In this thesis, both unlabeled and ^{13}C labeled Pep25 listed in Scheme 3 were synthesized. In addition, unlabeled and ^{13}C labeled Pep25 were dissolved in H_2O solution and ^{13}C isotope-edited IR spectroscopy was utilized to provide geometric information about the structure of Pep25 by ATR.

CHAPTER II

MATERIALS & METHODS

2.1 Peptide Synthesis

Peptides were synthesized via solid phase (Fmoc) chemistry (mechanism shown in Figure 12.[71-73] The procedure of Fmoc peptide synthesis comprises repeated cycles of coupling-washing-deprotection-washing (*cf.* Figure 12). During the coupling step, the amine group of the free amino acid in N,N-dimethylformide (DMF) solution is protected by Fmoc group and the carboxylic group is activated by diisopropylcarbodiimide (DIC). The activated carboxylic group will react with the amine group on the surface of the solid phase (i.e., Wang resin in this thesis) to form an amide bond. After the coupling, the remaining free Fmoc-protected amino acid in the DMF solution will be vented. The resin will be washed by fresh DMF to clean up the surface of solid phase. Then, piperidine DMF solution will be added to the reaction vessel to initiate the deprotection. During the deprotection step (cf. Figure 12), the Fmoc group which protects the amine group will react and link with piperidine. As a result, the amine group will be deprotected and ready to couple with the next amino acid. Thus, amino acids will be coupled onto the surface of Wang resin one by one to form a peptide, which will remain covalently attached to the surface of Wang resin until cleaved from it by a reagent such as trifluoroacetic acid (TFA).

Wang resin, Fmoc-protected amino acids, DIC, 1-hydroxylbenzotriazole, and piperidine were purchased from Anaspect Inc. (San Jose, CA). All the amino acids were in L-configuration, except glycine. The organic solvents (e.g., DMF, dichloromethane, ethyl ether, trifluoroacetic acid or TFA, and so on) for peptide synthesis were purchased from Thermo-Fisher Scientific Inc. (Pittsburgh, PA).

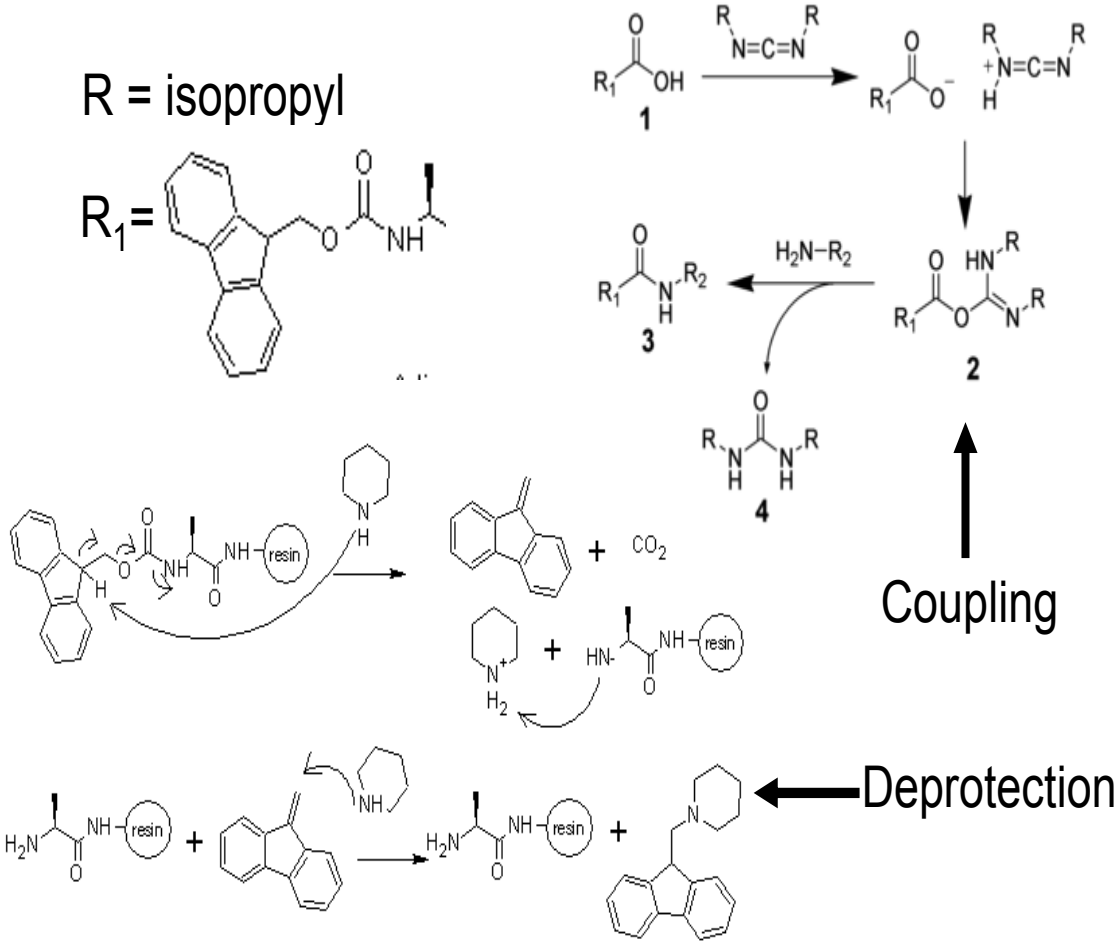

Figure 12: Organic mechanism of coupling and deprotection. R_2 is the resin linked with NH_2.

2.2 High Performance Liquid Chromatography (HPLC)

HPLC was performed using a solid support stationary phase (also called a "column"). The usual column contains unmodified silica particles, which is now called "normal phase chromatography". In normal phase chromatography, the stationary phase is hydrophilic and therefore has a strong affinity for hydrophilic molecules dissolved in the mobile phase. As a consequence, the hydrophilic molecules in the mobile phase tend to bind (or "adsorb") to the column and are eluted late. The hydrophobic molecules pass through the column more quickly and are eluted earlier. For the purification of peptides, reverse phase HPLC was utilized. The stationary phase of reverse phase HPLC is usually alkyl chains covered silica particles. Different to normal phase HPLC, hydrophilic molecules pass through the columns more quickly and are eluted earlier than hydrophobic molecules.

The crude peptides (both unlabeled and ^{13}C labeled) were purified by Waters 1525 HPLC (Milford, MA) equipped with 2489 UV-Vis detector (Figure 13) through a semi-preparative reversed-phase (RP) column (model Jupiter-00G-4055-P0 with 21.5 mm internal diameter and 250 mm length) from Phenomenex Inc. (Torrance, CA). The eluents were 0.1% trifluoroacetic acid in water (V/V, mobile phase A) and 0.1% trifluoroacetic acid in acetonitrile (V/V, mobile phase B). At a flow rate of 21.5 mL/min, purification of the peptides was accomplished with an elution gradient of 8–38% phase B for 35 minutes.

Figure 13: Waters 1525 HPLC system

2.3 Mass Spectroscopy

Mass spectrometry works by ionizing chemical compounds to generate charged molecules or molecule and measuring their mass-to-charge ratios. A mass spectrometer usually consists of three major components: ion source, mass analyzer, and detector. The ion source converts the sample into ions. An extraction system removes ions from the sample, which are then trajected through the mass analyzer and onto the detector. The mass analyzer will sort the ions of various molecules by the mass-to-charge ratio. The detector will provide data for calculating the abundances of each ion present.

All of the Mass measurements in this thesis were conducted on an Electrospray (ES) –Time of flight (TOF) (Waters Aqua model shown in Figure 14)

mass spectrometer (Milford, MA). Both labeled and unlabeled peptides were dissolved in water with 0.5 % trifluoroaceitic acid (TFA). Positive ion mode was used and the capillary voltage is 3 kV. Ion source temperature is 100 °C and N_2 gas of desolvation was blowed at 500 L/hour.

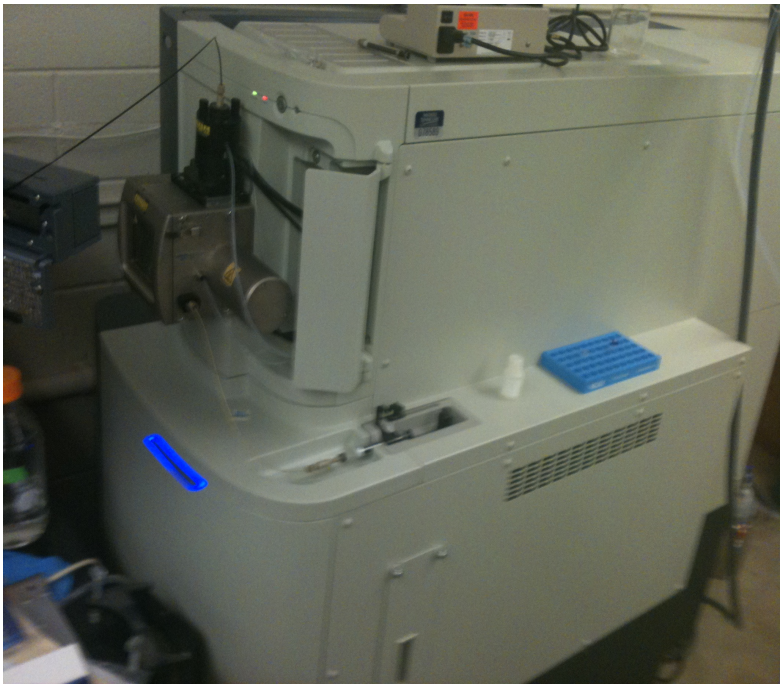

Figure 14: Waters Aqua time-of-flight (TOF) mass spectrometer.

2.4 Circular Dichroism (CD) Spectroscopy

Circular polarized light has two types: namely, left circular polarized (LCP) light rotating counter clockwise and right circular polarized (RCP) light rotating clockwise. CD refers to the difference in the absorption of LCP and RCP (Figure 15). If the LCP and RCP are absorbed to different extents by a sample

(such as peptides which contains chiral atoms), CD signal (ΔA) will result from the following equation:

$$\Delta A = A_L - A_R \qquad \text{Equation 2-1}$$

where ΔA is the difference between absorbance of LCP and RCP light. It can also be expressed by, applying Beer's law, as:

$$\Delta A = (\varepsilon_L - \varepsilon_R)Cb \qquad \text{Equation 2-2}$$

where ε_L and ε_R are the molar extinction coefficients for LCP and RCP light, C is the molar concentration and b is the path length in centimeters. Then,

$$\Delta\varepsilon = \varepsilon_L - \varepsilon_R \qquad \text{Equation 2-3}$$

Where $\Delta\varepsilon$ is the molar circular dichrosim. Although ΔA is usually measured as the CD signal, for historical reasons most measurements are reported in degree of ellipticity (molar ellipticity) whose units are degrees-cm^2/dmol.

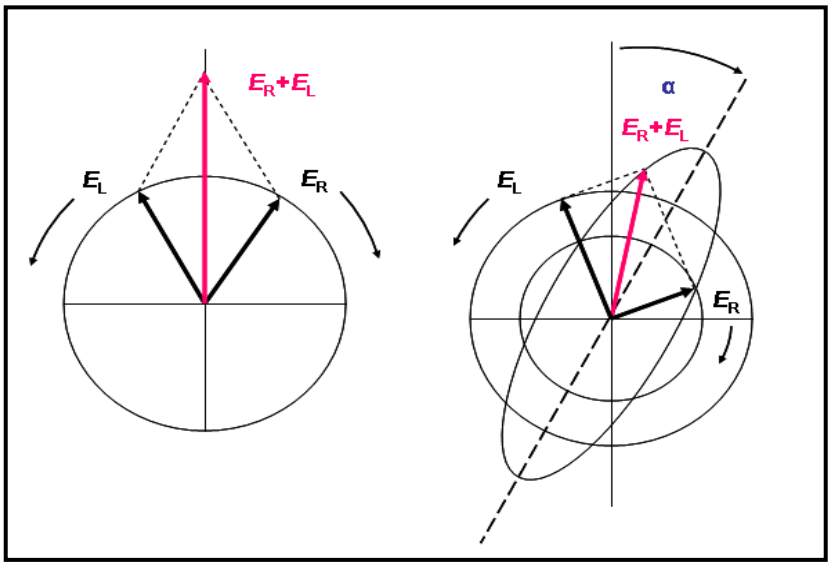

Figure 15**:** Diagrams showing how right and left circulatory polarized light combine (A) if two waves have the same amplitude, the result is plane-polarized

light. (B) if their amplitude differ, the result is elliptically polarized light, demonstrating the unequal contributions of right and left circular polarized light to give molar ellipticity (θ).

The circular dichroism (CD) spectra in this thesis were measured by a JASCO J-810 spectropolarimeter fitted with a 150-W xenon lamp (Figure 16). Quartz cells of 1 mm path length were used for all CD measurements and the spectra were recorded with a response time of 4 s and scan speed of 20 $nm \cdot min^{-1}$ with 2 measurement accumulation.

Figure 16: Jasco 810 CD spectrometer.

2.5 ATR FTIR Spectroscopy

Fourier transform infrared spectroscopy (FTIR) is a technique which is used to obtain an infrared absorption spectrum of a sample. Different to UV-Vis spectroscopy which shines a monochromatic beam on a sample, the incident beam of FTIR comprises lights with various wavelengths going through a sample simultaneously. The beam described above is generated by a broadband light source. Then, the lights shine into a Michelson interferometer (a set of mirrors, one of which is moved by a motor). Different wavelengths are modulated at different rates and the beam coming out of the interferometer depends on the position of the moving mirror. Computer processing is required to turn the raw data (light absorption for each moving mirror position) into the desired result (light absorption for each wavelength).

The FTIR spectra of labeled and unlabeled peptides aqueous solutions with concentration from 5 to 12 $mg \cdot ml^{-1}$ were measured by the EQUINOX 55 spectrometer with BioATR-cell II unit accessory (Figure 17) on the baseplate A729/q with a resolution of 4 cm^{-1} and coaddition of 128 scans. Pure water solution was used as the background for FTIR measurement.

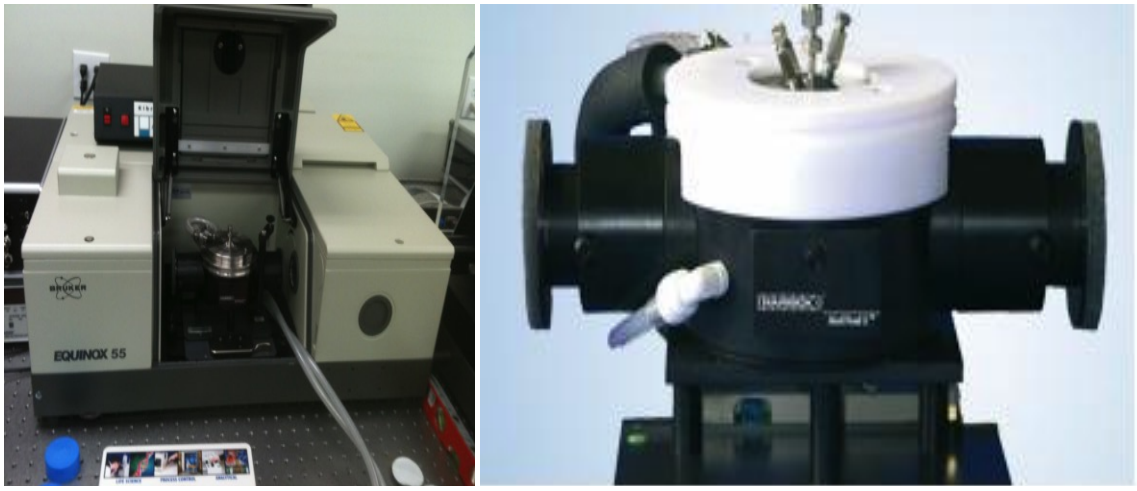

Figure 17: Equinox 55 spectrometer (left) and BioATR-cell II unit accessory (right)

CHAPTER III

RESULTS

3.1 HPLC Chromatograms of Unlabeled and Double ^{13}C Labeled Pep25

The HPLC chromatogram of unlabeled Pep25 is shown in Figure 18. The peak with a retention time of 20.0 minutes is unlabeled Pep25, which was confirmed by the Mass spectroscopy shown below. The HPLC chromatogram of the double ^{13}C labeled Pep25 is almost identical to that of unlabeled Pep25 and the result of ^{13}C labeled pep25 at residues at 12 and 13 (L1 in Scheme 2) is shown in Figure 19. The retention time of L1 is also 20.0 minutes and the relative peak intensity of other peaks is higher than those of unlabeled peptide (Figure 18). This indicates the increasing impurities, which may be because ^{13}C isotopic effect slows down the reaction rate of peptide synthesis and decrease the yield. HPLC chromatograms of other ^{13}C double labeled Pep25 (such as L2, L3 and L4) are identical to Figure 19.

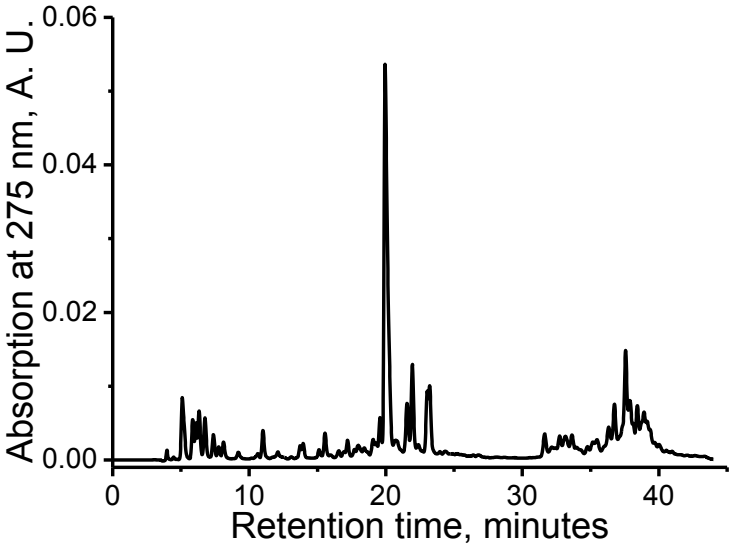

Figure 18: HPLC chromatogram of unlabeled Pep25

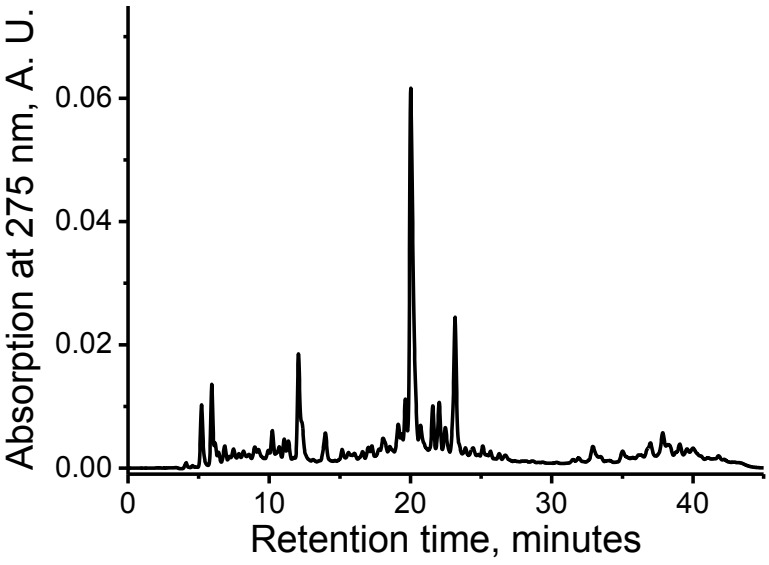

Figure 19: HPLC chromatogram ^{13}C labeled pep25 at residues 12 and 13 (L1).

3.2 Mass Spectra of Unlabeled and Labeled Pep25

The purified unlabeled Pep25 by HPLC was analyzed by Mass spectroscopy and the results are shown in Figure 20. The peak appearing at 1058.4 is assigned to the double protonated Pep25, whose theoretical molecular weight is 2115.3. The triple protonated Pep25 show the peak at 706.3 and the quarternarily protonated peak was at 529.7. As for double ^{13}C labeled Pep25 at 12 and 13 residues (e.g., L1 in Scheme 2), the double, triple, and quarternarily protonated peaks are at 1059.5, 706.9, and 530.2 respectively, (Figure 21) all of which correlate well to the theoretical value (i.e., 2117.3). The Mass spectra of L2, L3, and L4 are identical to that of L1 as shown in Figure 21.

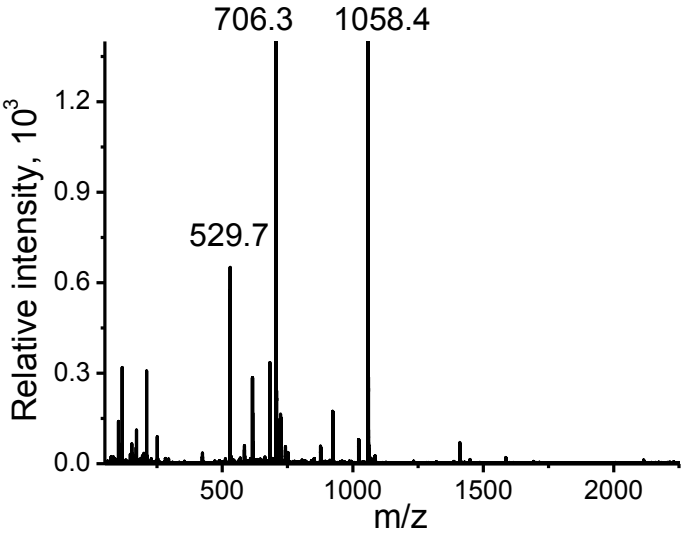

Figure 20: Mass spectrum of unlabeled Pep25

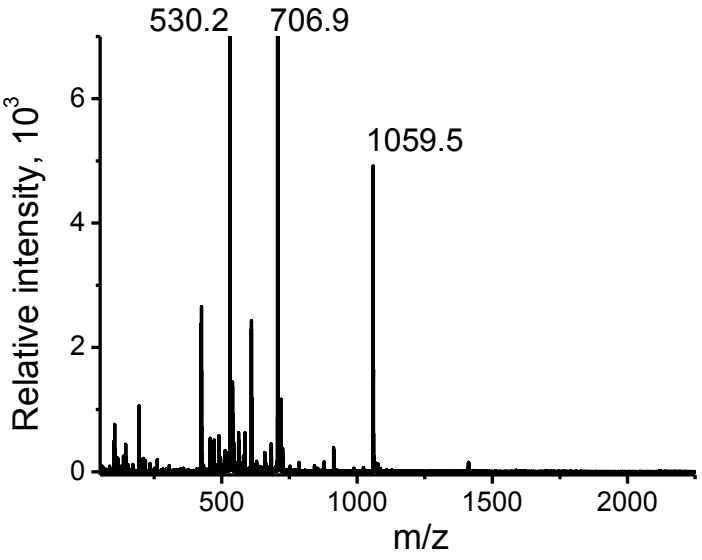

Figure 21: Mass spectrum of ^{13}C labeled at residues 12 and 13 (L1).

3.3 CD Spectrum of Pep25 at Different Temperatures

To determine the conformation of Pep25 at different temperatures, CD spectrum of Pep25 was measured and shown in Figure 22. At 10 °C, the CD spectrum of unlabeled Pep25 showed double negative peaks at 207 and 222 nm as well as a positive peak around 192 nm, all of which are characteristic peaks of helix. When the temperature was 45 °C, only one negative peak at 199 nm (the characteristic peak of unstructured conformation) was detected. Thus, Pep25 is in the helical conformation at 10 °C and transforms to unstructured conformation when the temperature increases to 45 °C. The CD spectra of double ^{13}C labeled Pep25 (e.g., L1, L2, L3, and L4) are identical to that of unlabeled Pep25 shown in Figure 22. This confirms that the double ^{13}C labels in Pep25 will not affect the conformation of Pep25.

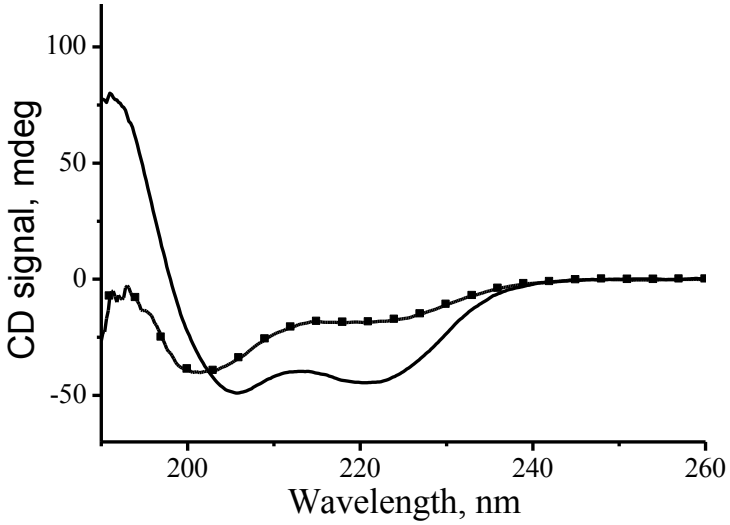

Figure 22: CD spectrum of unlabeled Pep25 at 10 °C (–) and 45 °C (-■-).

3.4 ATR FTIR Spectra of Pep25 at 10 °C in Phosphate Buffer at pH 7.4

The ATR FTIR spectra of both unlabeled and double ^{13}C labeled Pep25 at 10 °C were shown in Figure 23. As for unlabeled Pep25, amide I and amide II bands are detected at 1641 and 1550 cm^{-1}, respectively. As for L4 which the ^{13}C labels are at residues 9 and 13, both amide I and amide II bands were detected at very similar position as those of unlabeled Pep25 (*cf.,* Figure 23). Another peak at 1602 cm^{-1} was also detected. Because the only difference between unlabeled Pep25 and L4 is the presence of two ^{13}C labels in the carbonyls of residues 9 and 13, the peak at 1601 cm^{-1} is the ^{13}C amide I band of helix. As for L3 and L2, the ^{13}C amide I band of helix were detected at position of 1599 cm^{-1}. However, the ^{13}C amide I band shifted significantly to 1608 cm^{-1} for L1. On the other hand, it has been reported that the ^{13}C amide I band of unstructured

conformation is almost identical to the ^{12}C amide I band in D_2O.[56, 58] To verify the similar position of ^{13}C and ^{12}C amide I band of unstructured conformation in H_2O, the ATR FTIR spectra of Pep25 were measured with increasing temperature, which can change Pep25 from helix to unstructured conformation by the CD results shown in Figure 22.

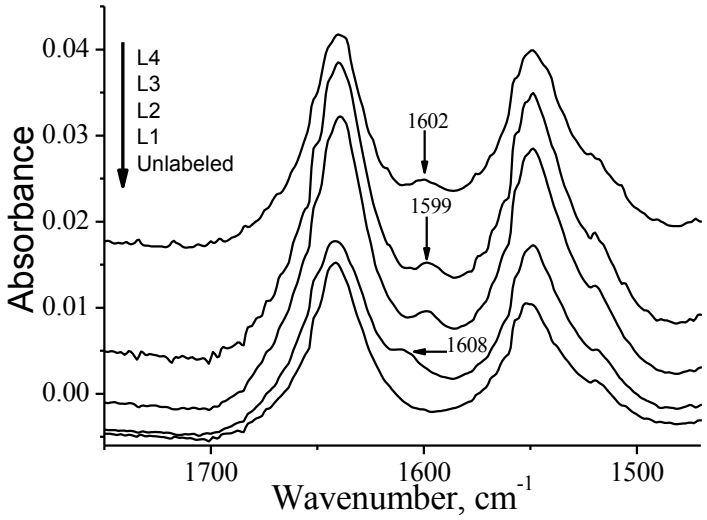

Figure 23: ATR FTIR spectra of unlabeled Pep25, L1, L2, L3, and L4 at 10 °C.

3.5. ATR FTIR Spectra of Pep25 at Various Temperatures

The ATR FTIR spectra of unlabeled Pep25, L1, and L3 are shown in Figure 24, 25, and 26, respectively. As shown in Figure 24, unlabeled Pep25 showed ^{12}C amide I band at 1641 cm^{-1} at 10 °C and the ^{12}C amide I band moved to 1644 cm^{-1} at 45 °C, under which Pep25 is unstructured shown by CD results (cf. Figure 22). As for L1, the ^{13}C amide I band of helix at 1608 cm^{-1} can be still

be detected at 15 °C but decreased with the increasing temperature as shown in Figure 25. When the temperature increased to 45 °C, the peak disappeared completely. Similarly, the ^{13}C amide I band of L3 at 1599 cm^{-1} also disappeared when the temperature increased to 45 °C (*cf.* Figure 26). Similar to Figure 25 and 26, the ^{13}C amide I band of the FTIR spectra of L2 and L4 also disappeared with increasing temperature (results not shown). This indicates that the difference between the ^{13}C and ^{12}C amide I band of unstructured conformation may be too minor to be detected.

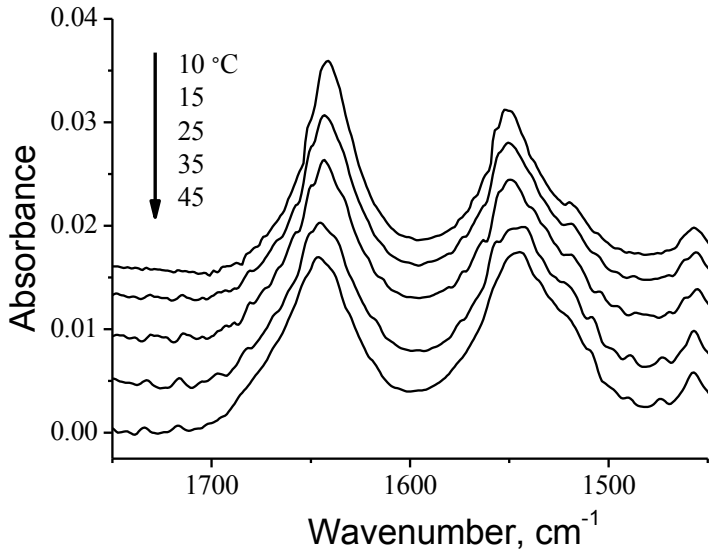

Figure 24: The ATR FTIR spectra of unlabeled Pep25 under various temperatures in phosphate buffer at pH 7.4.

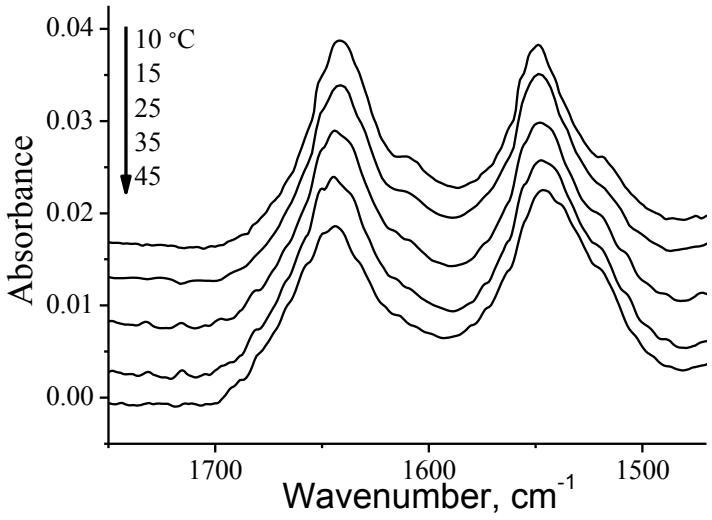

Figure 25: The ATR FTIR spectra of L1 under various temperatures in phosphate buffer at pH 7.4.

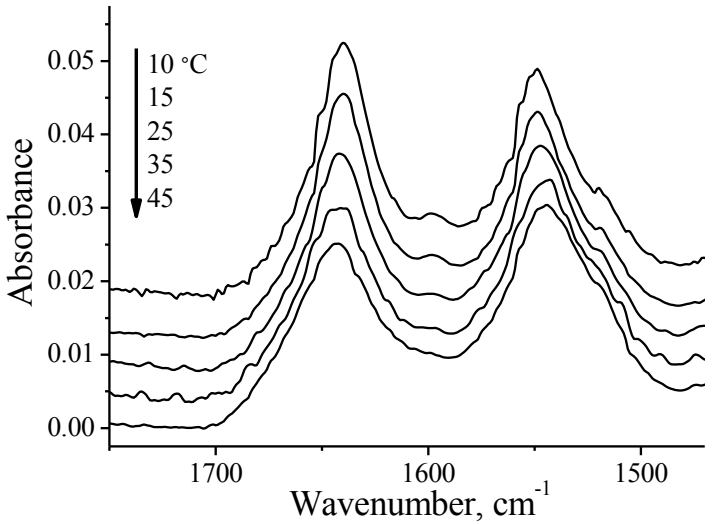

Figure 26: The ATR FTIR spectra of L4 under various temperatures in phosphate buffer at pH 7.4.

CHAPTER IV

DISCUSSION & CONCLUSION

4.1 Presence of Amide II Band

As mentioned in Chapter 1, amide II band is the bending mode vibration of N-H. In D_2O, amide II band moves to ~1400 cm^{-1} because of the higher atomic weight of deuterium atom. As shown in Figure 23 to 26, the amide II band appears around 1545 cm^{-1}, which is the normal position in H_2O. This is a clear evidence of the success of the measurement of FTIR spectra of Pep25 in H_2O by ATR. However, the gap between amide I band and amide II band is smaller in H_2O than that in D_2O. If amide II band covers the ^{13}C amide I band from ^{13}C labels, the detection of ^{13}C amide I band will be difficult and it is impossible to apply ^{13}C isotope edited FTIR in H_2O.

4.2 ^{13}C Amide I Band of ^{13}C Labeled Residues in Unstructured Conformation

Theoretically, ^{13}C labeled residues will downshift the peak position even for a residue in unstructured conformation. However, in Figure 25 and 26, no ^{13}C amide I band was detected in the FTIR spectra of all the ^{13}C labeled Pep25 (i.e., L1, L2, L3, and L4), when the temperature increased to 45 °C at which both of the peptides are in unstructured conformation. This may be due to the fact that solvent (i.e., H_2O) molecules interact with peptide more in unstructured

conformation and the carbonyls in unstructured conformation are surrounded by H_2O molecules. This will delocalize the C=O stretching and decrease the downshifting effect of ^{13}C labels. Consequently, the difference between the ^{12}C and ^{13}C amide I band in unstructured conformation may be too small to be detected.

4.3 ^{13}C Amide I Band of ^{13}C Labeled Residues in α-helix

Different to residues in unstructured conformation, carbonyls in α-helix form strong intra-molecular H-bonds. Thus, solvent H_2O molecules do not interact with the carbonyls in α-helix as much and the ^{13}C labels will downshift the ^{13}C amide I band substantially. However, if the ^{13}C amide I band was downshifted too much and is covered by the amide II band, the detection of the ^{13}C amide I band would be difficult and the application of ^{13}C isotope edited FTIR technique in H_2O would be challenging. Fortunately, all the ^{13}C amide I bands of α-helix appear around 1600 cm^{-1}, which is just in the middle of amide I and amide II bands (cf., Figure 25 and 26). Since the background absorbance from unlabeled pep25 is weak at 1602 cm^{-1} (*cf.* Figure 23 and 24), the peak at 1602 cm^{-1} will be easy to detect. The good position of the ^{13}C amide I band of α-helix at 1602 cm^{-1} makes it probable for the further application of ^{13}C isotope edited FTIR technique in H_2O promising. It has been suggested that the ^{13}C amide I band might be covered by amide I or II band.[74] Here, we clearly show that ^{13}C amide I band is not covered by amide I or II band and can be clearly detected.

4.4 Relationship Between ^{13}C Amide I Band Position and Geometry of Helix

As mentioned in Figure 22, Pep25 is in the helical conformation in H_2O at pH 7.4 at 10 °C. The regular (^{12}C) amide I band position of helical conformation has been shown to usually be around 1650 cm^{-1}, which is different to that (at 1641 cm^{-1}) of Pep25 shown in Figure 24. It is worth noting that the ^{12}C amide I band position of helical structure has been reported to be detected at positions different from the usual one (i.e., 1650 cm^{-1}). On the other hand, the amide I band of helical structure in H_2O is usually ~6 cm^{-1} higher than that in D_2O. Notice that the ^{12}C amide I band position of helical Pep25 in D_2O was detected at 1635cm^{-1}. Thus, the ^{12}C amide I band of Pep25 at 1641 cm^{-1} in Figure 24 is reasonable.

Similarly, the ^{13}C amide I band position of L1, L2, L3, and L4 in D_2O has been reported to be at 1600, 1592, 1590, 1596 cm^{-1},[56, 58] respectively, all of which are around 6 cm^{-1} lower than the corresponding position in H_2O shown in Figure 24-26 (1608 cm^{-1} for L1, 1599 cm^{-1} for L2, 1599 cm^{-1} for L3, and 1602 cm^{-1} for L4). Thus, the ^{13}C amide I band position of Pep25 in H_2O is also reasonable. In addition, the ^{13}C amide I band position is also related to the spacer residues between the two labeled ones, which has been reported in D_2O. Therefore, the geometry information about the structure of peptides/proteins in H_2O can be investigated by ^{13}C isotope-edited ATR FTIR spectroscopy.

4.5 D_2O Effect on the Structure and Biophysical Properties of Proteins

Since D_2O is often used as solvent in the study (such as NMR) of proteins, there has been a long time running argument about the affect of D_2O on the structure of proteins. Fisher et al. have reported that substitution of hydrogen by deuterium (i.e., H/D exchange) can only cause subtle change in the structure of proteins.[60] On the other hand, Sanchez-Gonzalez and co-authors have shown that H/D exchange causes substantial change in the proteins structure of fish surimi.[75] In addition, it has been reported that H/D exchange cause changes in the stability of some globular proteins.[62] In this work, no significant difference between Pep25 in H_2O from that in D_2O was detected.

4.6 Conclusion

Unlabeled and double ^{13}C labeled Pep25 were synthesized. The Pep25 samples were confirmed by Mass spectroscopy and purified by reverse phase HPLC. Pep25 is in unstructured conformation at 45 °C whereas transforms to α-helix at 10 °C. No difference was detected between the regular (^{12}C) and ^{13}C amide I band in unstructured conformation. However, the peak of ^{13}C labeled residues in α-helix appears around 1602 cm^{-1}, which can be used as a fingerprint peak of α-helix for specifically ^{13}C labeled residues. In addition, the ^{13}C amide I band position is related to the number of spacing residues between the two ^{13}C labels. For example, when the two ^{13}C labels are adjacent (the spacing residue

number is zero), the ^{13}C amide I band was detected at 1608 cm^{-1}. When the number of spacing residues is 1, 2, and 3, the ^{13}C amide I band was detected at 1599, 1599, and 1602 cm^{-1}, respectively. Therefore, the geometric information about the structure of helix can be provided by the ^{13}C amide I band position in H_2O by ATR ^{13}C isotope-edited FTIR spectroscopy.

CHAPTER V

FUTURE WORK

5.1 ^{13}C Isotope-edited FTIR to Determine the Structure of Peptide in β-sheet

Clarification of protein structure is important to correlate the function of a protein with its structure and X-ray crystallography is a powerful technique to elucidate the protein structure in atomic level. However, many proteins cannot form single crystals, hampering such analysis. β-Amyloid (Aβ), which contains 40–42 amino acids, is one such non-crystalline protein. Abnormal aggregation of Aβ is responsible for Alzheimer's diseases (AD), [76] which is the most common neurodegenerative disease and affects more than five million people in US.[77] Aβ aggregates can be divided to two types, namely, mature fiber and oligomer (the early aggregate stage),[76] both of which are in β-sheet conformation. The structure of Aβ fiber and oligomer has been reported to be important for drug development for AD treatment.[22, 78] Therefore, efforts have been carried out to elucidate the structure of both Aβ aggregates.

NMR has been shown to be another powerful technique to determine the structure of Aβ aggregates. As for mature fiber, solid-state NMR showed that the first eight N-terminus residues as well as several C-terminal residues are unstructured in the mature fiber.[79] Furthermore, Tycko et al. reported that several

residues in the middle of Aβ sequence (G25, S26, and G29) may be also in unstructured conformation in mature fiber.[80] Interestingly, Dupree and coworkers have introduced ^{15}N and ^{17}O labeled residues into Aβ sequence and obtained more detailed information about the structure of Aβ mature fiber.[80]

Different to mature fiber, Aβ oligomer has been reported to be cytotoxic and probably responsible for the neuronal cells death in the brain of AD patients.[16, 17, 81-89] However, only limited results have been obtained about the Aβ oligomer structure by NMR. For example, an intra-residue contact between E22 and I31 was detected in Aβ oligomer by NMR.[31] The difficulty may be because the NMR measurement of peptides/proteins is usually time intensive (over ten hours) whereas the lifetime of Aβ oligomer is only about one to several hours. Another challenge of NMR measurement is the nature of heterogeneity of Aβ oligomer. Although soluble in water, the hydrophobic core of Aβ oligomer does not dissolve well in H_2O. Therefore, although the atomic-resolution dynamics of the surface of Aβ oligomer has addressed recently by NMR,[33] the information about the hydrophobic core of Aβ oligomer may be difficult to elucidate by NMR.

Recently, structural information about the Aβ mature fiber has been also obtained by ^{13}C isotope-edited FTIR spectroscopy. As for β-sheet, the regular (^{12}C) amide I band of β-sheet conformation appears at 1630 cm^{-1} in H_2O solution and decreases to 1620 cm^{-1} in D_2O solution because of the H/D exchange. In β-sheet, the hydrogen bond forms between the amide groups in neighboring strands (as shown in Scheme 4A).[55] The ^{13}C labeled residue has been reported to decrease the amide I band in D_2O to 1600 cm^{-1} when forming an H-bond with regular ^{12}C

residues (Scheme 4B),[55, 57, 90, 91] which was called ^{13}C-^{12}C coupling. If both neighboring residues contain ^{13}C labels (Scheme 4C), a strong ^{13}C-^{13}C coupling occurs and the ^{13}C amide I band will further decrease to 1590 cm^{-1}, which can be used to address the structure of peptides in β-sheet as below.[55, 57, 90, 91]

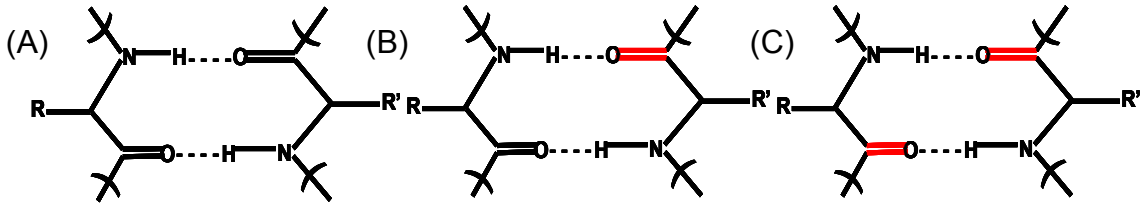

Scheme 4. Hydrogen bond formation between the amide groups in neighboring strands of β-sheet. The atoms in red are ^{13}C labels.

Segment peptide of Aβ containing residues 16 to 22 (Aβ(16–22)) has been shown to form fibers in β-sheet conformation similar to those of whole Aβ protein.[55, 76] ^{13}C labels were introduced to carbonyls of different residues to clarify the structure of Aβ(16–22) fiber. When residue 17, 18, 20, and 21 is labeled individually, the amide I band was detected at 1600 cm^{-1},[55, 57] which is the ^{13}C-^{12}C coupling and the labeled residues are packed as shown in Scheme 5A in the fiber. When F19 is labeled by ^{13}C individually, the amide I band decreased to 1590 cm^{-1}, which is the ^{13}C-^{13}C coupling. F19 should be the central residue in the fiber as shown in Scheme 5B. In addition, residue 17 and 21 were labeled simultaneously and the peak at 1590 cm^{-1} was also detected. Therefore, residue 17 and 21 should be coupled in the neighbor strands of the anti-parallel β-sheet structure in the fiber as shown in Scheme 5C. By this method, all of the

remaining residues can be screened by introducing double ^{13}C labels simultaneously and the structure of the Aβ(16–22) fiber can be elucidated in residue level.[55, 57]

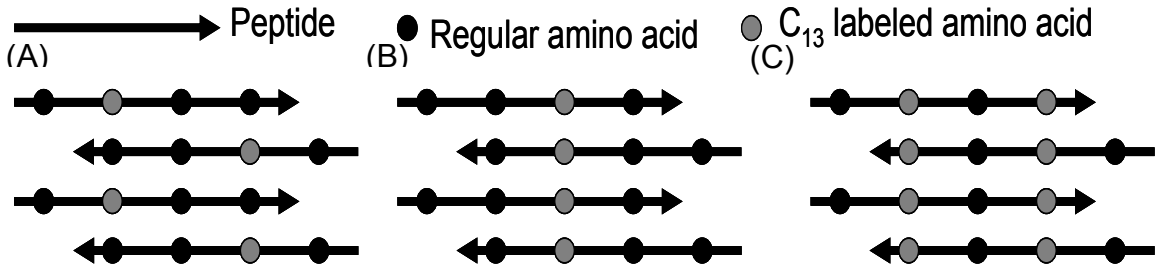

Scheme 5: Diagram showing ^{13}C labeled residue at different positions. (A) The ^{13}C labeled amino acid is not the central residue of Aβ(16–22) fibers. (B) A strong ^{13}C-^{13}C coupling will arise when the ^{13}C labeled residue is the central residue of Aβ(16–22) fibers. (C) Determining the structure of Aβ(16–22) fibers in residue level by the double ^{13}C labeled amino acids.

Again, it is worth noting that all of the measurements of ^{13}C isotope-edited FTIR spectroscopy were in D_2O, which is not a physiological solvent. In addition, H_2O has been reported to be extensively involved in the aggregation pathway of amyloidogenic proteins.[92] Furthermore, the techniques (such as cytotoxicity and Western blot) to determine the formation of Aβ oligomer can only work in H_2O, not D_2O. Therefore, application of ^{13}C isotope-edited FTIR in H_2O to determine the structure of peptides/proteins will be important.

5.2 Synthesis of Unlabeled and ^{13}C Labeled Aβ(16–22) Peptides

Unlabeled Aβ(16–22) peptide (i.e., KLVFFAE) has been synthesized successfully and the Mass spectrum of crude sample is shown in Figure 27. The theoretical mass of Aβ(16–22) is 852.6. Thus, the peak at 853.6 in Figure 27 is the mono-protonated peak of Aβ(16–22). The other peaks in the spectrum are assigned to impurities, which have been detected by the HPLC chromatogram shown in Figure 28. We also incubated the Aβ(16–22) peptide to form mature fiber successfully as shown in Figure 29.

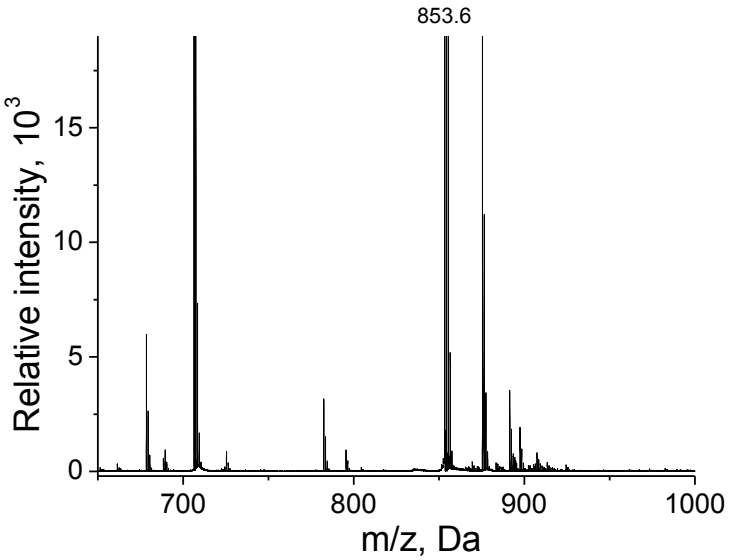

Figure 27: Mass spectrum of unlabeled Aβ(16–22).

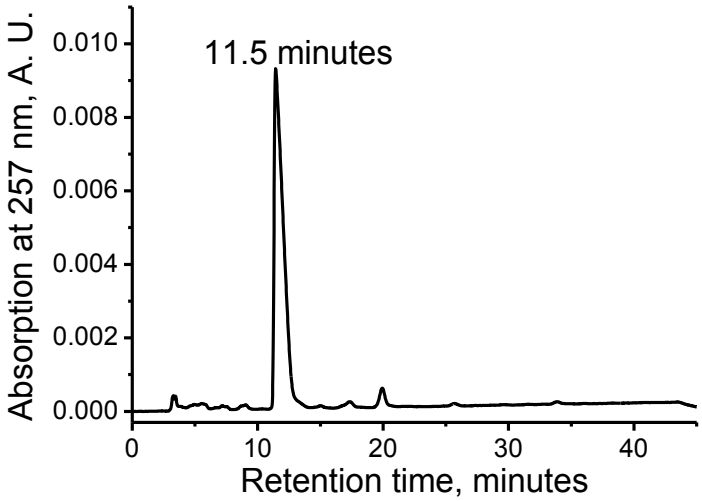

Figure 28: HPLC chromatogram of unlabeled Aβ(16–22).

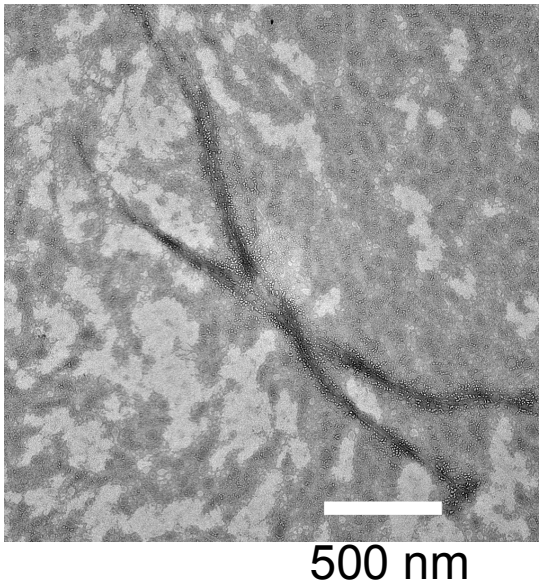

Figure 29: TEM image of the mature fiber of Aβ(16–22).

5.3 Future Work Including the Synthesis of ^{13}C Labeled Aβ(16–22) Peptides and ATR FTIR Spectroscopy of Aβ(16–22) Mature Fiber as well as Oligomer

First, single ^{13}C labeled residue will be introduced to Aβ(16–22) as shown in Scheme 6 from L-S1 to L-S7. The labeled Aβ(16–22) will be incubated in H_2O at pH 7.4 in phosphate buffer to form mature fiber, which will be monitored by thioflavin T (ThT) fluorescence, scanning electric micrograph (SEM) technique, and CD spectroscopy. Then, the fiber will be analyzed by ATR FTIR spectroscopy.

Similar to the results shown above in Scheme 4, two type of ^{13}C amide I band will be observed. If the ^{13}C labeled residue is packed to regular residue as shown in Scheme 5A, **^{13}C-^{12}C coupling** will occur. If the ^{13}C labeled residue is neighboring to another ^{13}C labeled residue in the next Aβ(16–22) packed in the fiber (*cf.* Scheme 5B), the **^{13}C-^{13}C coupling** will be detected and the ^{13}C amide I band will be further downshift. In the case shown in Scheme 5B, the ^{13}C labeled residue is central in the fiber. Then, the two residues adjacent to the central residue will be ^{13}C labeled simultaneously. For example, if F19 is the central residue, V18 and F20 will be ^{13}C labeled at the same time as L-D1 in Scheme 6. ATR FTIR spectrum of this double ^{13}C labeled mature fiber will be also measured to confirm that V18 and F20 are packed as shown in Scheme 5C by the presence of amide I peak of ^{13}C-^{13}C coupling. Similarly, double ^{13}C labels will be also introduced to L17&A21 (L-D2 in Scheme 6) or K16&E22 (L-D3 in Scheme 6). The

ATR-FTIR spectroscopy of mature fiber of L-D2 or L-D3 will be also studied to confirm that L17&A21 or K16&E22 are arranged as Scheme 5C by the presence of ^{13}C-^{13}C coupling.

NH_2-K̲LVFFAE-Ac (L-S1)
NH_2-KL̲VFFAE-Ac (L-S2)
NH_2-KLV̲FFAE-Ac (L-S3)
NH_2-KLVF̲FAE-Ac (L-S4)
NH_2-KLVFF̲AE-Ac (L-S5)
NH_2-KLVFFA̲E-Ac (L-S6)
NH_2-KLVFFAE̲-Ac (L-S7)
NH_2-KLV̲FF̲AE-Ac (L-D1)
NH_2-KL̲VFFA̲E-Ac (L-D2)
NH_2-K̲LVFFAE̲-Ac (L-D3)

Scheme 6: Sequence of the ^{13}C labeled Aβ(16–22) peptides. The carbonyls of underlined residues are replaced by ^{13}C labels.

Aβ oligomer, which is still in β-sheet conformation, has been reported to be the early stage of the aggregation process.[93, 94] As presented in section **5.1**, another major difference between Aβ mature fiber and oligomer is that oligomer is cytotoxic. Thus, all of the single ^{13}C labeled Aβ(16–22) peptides shown in Scheme 6 will be incubated in phosphate buffer at pH 7.4 to form of Aβ(16–22) oligomer, which will be monitored by CD spectroscopy together with cytotoxicity assay. The formation of Aβ(16–22) oligomer will cause the cytotoxicity as well as the characteristic peaks of β-sheet in CD spectra. In addition, Aβ(16–22) oligomer usually will not induce the fluorescence of ThT. The H_2O solution of Aβ(16–22) oligomer will be analyzed by ATR-FTIR spectroscopy. The ^{13}C amide

I band of ^{13}C-^{12}C and ^{13}C-^{13}C coupling in H_2O determined in mature fiber of Aβ(16–22) will be used to address the structure of Aβ(16–22) oligomer. In general, Aβ(16–22) will be used as a model peptide to build up the methodology of ^{13}C isotope-edited FTIR spectroscopy to address the structure of peptides/proteins in β-sheet conformation.

REFERENCES

1. Kobko, N.; Paraskevas, L.; del Rio, E.; Dannenberg, J., Cooperativity in amide hydrogen bonding chains: Implications for protein-folding models. *J. Am. Chem. Soc.* **2001,** 123, 4348-4349.

2. Lam, R. S. H.; Nickerson, M. T., Food proteins: A review on their emulsifying properties using a structure-function approach. *Food Chem.* **2013,** 141, 975-984.

3. Peters, D.; Peters, J., Structure and bonding in proteins: Electron organization in amide unit. *J. Mol. Struct.* **1978,** 50, 133-145.

4. Sachs, J. N.; Engelman, D. M., Introduction to the membrane protein reviews: The interplay of structure, dynamics, and environment in membrane protein function. *Ann. Rev. Biochem.* **2006,** 75, 707-712.

5. Greenwald, R. A., Superoxide-dismutase and catalase as therapeutic agents for human diseases, a critical review. *Free Radical Biol. Med.* **1990,** 8, 201–209.

6. Loredo-Trevino, A.; Gutierrez-Sanchez, G.; Rodriguez-Herrera, R.; Aguilar, C. N., Microbial enzymes involved in polyurethane biodegradation: A review. *J. Polymers Envir.* **2012,** 20, 258-265.

7. Srikanth, K.; Pereira, E.; Duarte, A. C.; Ahmad, I., Glutathione and its dependent enzymes' modulatory responses to toxic metals and metalloids in fish-a review. *Environ. Sci. Pollut. Res.* **2013,** 20, 2133-2149.

8. Testa, B.; Pedretti, A.; Vistoli, G., Foundation review: Reactions and enzymes in the Metabolism of drugs and other Xenobiotics. *Drug Disc. Today* **2012,** 17, 549-560.

9. Wevers, R. A.; de Rijk-van Andel, J. F.; Brautigam, C.; Geurtz, B.; van den Heuvel, L.; Steenbergen-Spanjers, G. C. H.; Smeitink, J. A. M.; Hoffmann, G. F.; Gabreels, F. J. M., A review of biochemical and molecular genetic aspects of tyrosine hydroxylase deficiency including a novel mutation (291delC). *J. Inherited Metabolic Dis.* **1999**, 364–373.

10. McCauley, M. J.; Williams, M. C., Review: Optical tweezers experiments resolve distinct modes of DNA-protein binding. *Biopolymers* **2009,** 91, 265-282.

11. Dubnau, D., Binding and transport of transforming DNA by Bacillus subtilis: The role of type-IV pilin-like proteins - A review. *Gene* **1997,** 192, 191-198.

12. Appert-Collin, A.; Baisamy, L.; Diviani, D., Review - Regulation of G protein-coupled receptor signaling by A-kinase anchoring proteins. *J. Receptors Sign. Trans.* **2006,** 26, 631-646.

13. Mizejewski, G. J., Review of the putative cell-surface receptors for alpha-fetoprotein: Identification of a candidate receptor protein family. *Tumor Biol.* **2011,** 32, 241-258.

14. Chautard, E.; Thierry-Mieg, N.; Ricard-Blum, S., Interaction networks: From protein functions to drug discovery. A review. *Path. Biol.* **2009,** 57, 324-333.

15. Smythies, J.; Galzigna, L., The oxidative metabolism of catecholamines in the brain: A review. *Biochim. Biophys. Acta.* **1998,** 1380, 159–162.

16. Varadarajan, S.; Yatin, S.; Aksenova, M.; Butterfield, D. A., Review: Alzheimer's amyloid β-peptide-associated free radical oxidative stress and neurotoxicity. *J. Struct. Biol.* **2000,** 130, 184−208.

17. Wright, J. A.; Brown, D. R., Alpha-synuclein and its role in metal binding: Relevance to Parkinson's disease. *J. Neurosci. Res.* **2008,** 86, 496−503.

18. Deisenhofer, J.; Epp, O.; Miki, K.; Huber, R.; Michel, H., Structure of the protein subunits in the photosynthetic reaction centre of Rhodopseudomonas viridis at 3Å resolution. *Nature* **1985,** 318, 918-924.

19. Petry, S.; Brodersen, D. E.; Murphy, F. V.; Dunham, C. M.; Selmer, M.; Tarry, M. J.; Kelley, A. C.; Ramakrishnan, V., Crystal structures of the ribosome in complex with release factors RF1 and RF2 bound to a cognate stop codon. *Cell* **2005,** 123, 1255-1266.

20. Pfister, P.; Corti, N.; Hobbie, S.; Bruell, C.; Zarivach, R.; Yonath, A.; Bottger, E. C., 23S rRNA base pair 2057-2611 determines ketolide susceptibility and fitness cost of the macrolide resistance mutation 2058A -> G. *Proc. Natl. Acad. Sci. U. S. A.* **2005,** 102, 5180-5185.

21. Steitz, T. A., A structural understanding of the dynamic ribosome machine. *Nat. Rev. Mol. Cell Biol.* **2008,** 9, 242-253.

22. Adessi, C.; Soto, C., Beta-sheet breaker strategy for the treatment of Alzheimer's disease. *Drug Development Res.* **2002,** 56, 184−193.

23. Pauling, L.; Corey, R. B., Configurations of polypeptide chains with favored orientations around single bonds. *Proc. Nat. Acad. Sci. U.S.A.* **1951,** 37, 729−740.

24. Wang, C.; Shah, N.; Thakur, G.; Zhou, F.; Leblanc, R. M., α-Synuclein in α-helical conformation at the air-water interface: Implication of conformation and orientation changes during its accumulation/aggregation. *Chem. Commun.* **2010,** 46, 6702–6704.

25. Floudas, C. A.; Fung, H. K.; McAllister, S. R.; Monnigmann, M.; Rajgaria, R., Advances in protein structure prediction and de novo protein design: A review. *Chem. Engin. Sci.* **2006,** 61, 966-988.

26. Robinson, N. E.; Robinson, A. B., Review article: Use of Merrifield solid phase peptide synthesis in investigations of biological deamidation of peptides and proteins. *Biopolymers* **2008,** 90, 297-306.

27. Kahn, R.; Carpentier, P.; Berthet-Colominas, C.; Capitan, M.; Chesne, M. L.; Fanchon, E.; Lequien, S.; Thiaudiere, D.; Vicat, J. Z., P.; Stuhrmann, H., Feasibility and review of anomalous X-ray diffraction at long wavelengths in materials research and protein crystallography. *J. Synchront. Rad.* **2000,** 7, 131-138.

28. Lanyi, J. K., X-ray diffraction of bacteriorhodopsin photocycle intermediates (Review). *Mol. Membrane Biol.* **2004,** 21, 143-150.

29. Munte, C. E.; Erlach, M. B.; Kremer, W.; Koehler, J.; Kalbitzer, H. R., Distinct conformational states of the Alzheimer -amyloid peptide can be detected by high-pressure NMR spectroscopy. *Angew. Chem.* **2013,** 52, 8943-8947.

30. Comellas, G.; Rienstra, C. M., Protein structure determination by magic-angle spinning solid-state NMR, and Insights into the formation, structure, and stability of amyloid fibrils. *Ann. Rev. Biophys.* **2013,** 42, 515-536.

31. Scheidt, H. A.; Morgado, I.; Huster, D., Solid-state NMR reveals a close structural relationship between amyloid-β protofibrils and oligomers. *J. Biol. Chem.* **2012,** 287, 22822-22826.

32. Scheidt, H. A.; Morgado, I.; Rothemund, S.; Huster, D., Dynamics of amyloid beta fibrils revealed by solid-state NMR. *J. Biol. Chem.* **2012,** 287, 2017-2021.

33. Fawzi, N. L.; Ying, J. F.; Ghirlando, R.; Torchia, D. A.; Clore, G. M., Atomic-resolution dynamics on the surface of amyloid-beta protofibrils probed by solution NMR. *Nature* **2011,** 480, 268-U161.

34. Aronoff-Spencer, E.; Burns, C. S.; Avdievich, N. I.; Gerfen, G. J.; Peisach, J.; Antholine, W. E.; Ball, H. L.; Cohen, F. E.; Prusiner, S. B.; Millhauser, G. L., Identification of the Cu^{2+} binding sites in the N-terminal domain of the prion protein by EPR and CD spectroscopy. *Biochemistry* **2000,** 39, 13760−13771.

35. Ji, X.; Zheng, J.; Xu, J.; Rastogi, V. K.; Cheng, T.; DeFrank, J. J.; Leblanc, R. M., (CdSe)ZnS quantum dots and organophosphorus hydrolase bioconjugate as biosensors for detection of paraoxon. *J. Phys. Chem. B* **2005,** 109, 3793−3799.

36. Constantine, C. A.; Gattas-Asfura, K. M.; Mello, S. V.; Crespo, G.; Rastogi, V.; Cheng, T.; De Frank, J. J.; Leblanc, R. M., Layer-by-layer films of chitosan, organophosphorus hydrolase and thioglycolic acid-capped CdSe quantum dots for the detection of paraoxon. *J. Phys. Chem. B* **2003,** 107, 13762−13764.

37. Sreerama, N.; Woody, R. W., Estimation of protein secondary structure from CD spectra: Comparison of CONTIN, SELCON and CDSSTR methods with an expanded reference set. *Anal. Biochem.* **2000,** 282, 252–260.

38. Wang, C.; Micic, M.; Ensor, M.; Daunert, S.; Leblanc, R. M., Infrared reflection-absorption spectroscopy and polarization-modulated infrared reflection-absorption spectroscopy studies of the aequorin Langmuir monolayer. *J. Phys. Chem. B* **2008,** 112, 4146–4151.

39. Wang, C.; Zheng, J.; Zhao, L.; Rastogi, V. K.; Shah, S. S.; DeFrank, J. J.; Leblanc, R. M., Infrared reflection-absorption spectroscopy and polarization-modulated Infrared Reflection-Absorption Spectroscopy studies of the organophosphorus acid anhydrolase Langmuir monolayer. *J. Phys. Chem. B* **2008,** 112, 5250–5256.

40. Hasegawa, T.; Nishijo, J.; Watanabe, M.; Umemura, J.; Ma, Y.; Sui, G.; Huo, Q.; Leblanc, R. M., Characteristics of long-chain fatty acid monolayers studied by infrared external-reflection spectroscopy. *Langmuir* **2002**, 12, 4758–4764.

41. Thakur, G.; Leblanc, R. M., Conformation of lysozyme Langmuir monolayer studied by Infrared Reflection Absorption Spectroscopy. *Langmuir* **2009,** 25, 2842–2849.

42. Thakur, G.; Micic, M.; Leblanc, R. M., Surface chemistry of Alzheimer's disease: A Langmuir monolayer approach *Colloid. Surf. B* **2009,** 74, 436–456.

43. Wang, C.; Zheng, J.; Oliveira, O. N.; Leblanc, R. M., Nature of the interaction between a peptidolipid Langmuir monolayer and paraoxon in the subphase. *J. Phys. Chem. C* **2007,** 111, 7826−7833.

44. Du, X.; Miao, W.; Liang, Y., IRRAS studies on chain orientation in the monolayers of amino acid amphiphiles at the air-water interface depending on metal complex and hydrogen bond formation with the headgroups. *J. Phys. Chem. B* **2005,** 109, 7428−7434.

45. Jiang, D.; Dinh, K. L.; Tuthenburg, T. C.; Zhang, Y.; Su, L.; Land, D. P.; Zhou, F., A kinetic model for β-amyloid adsorption at the air/solution interface and its implication to the β-amyloid aggregation process. *J. Phys. Chem. B* **2009,** 113, 3160−3168.

46. Dziri, L.; Desbat, B.; Leblanc, R. M., Polarization-modulated FT-IR spectroscopy studies of acetylcholinesterase secondary structure at the air-water interface. *J. Am. Chem. Soc.* **1999,** 121, 9618-9625.

47. Hasegawa, T.; Moriya, D.; Kakuda, H.; Li, C.; Orbulescu, J.; Leblanc, R. M., Fibril-like aggregate formation of peptide carboxylate Langmuir films analyzed by surface pressure, surface dipole moment, and infrared spectroscopy. *J. Phys. Chem. B* **2005,** 109, 12856-12860.

48. Zheng, J. Y.; Constantine, C. A.; Zhao, L.; Rastogi, V. K.; Cheng, T. C.; DeFrank, J. J.; Leblanc, R. M., Molecular interaction between organophosphorus acid anhydrolase and diisopropylfluorophosphate. *Biomacromolecules* **2005,** 6, 1555-1560.

49. Dong, A.; Huang, P.; Caughey, W., Redox-dependent changes in β-extended chain and turn structures of cytochrome c in water solution determined by second derivative amide I infrared spectra. *Biochemistry* **1992,** 31, 182-189.

50. Halverson, K. J.; Sucholeiki, I.; Ashburn, T. T.; Lansbury, P. T., Location of β-sheet-forming sequences in amyloid proteins by FTIR. *J. Am. Chem. Soc.* **1991,** 113, 6701-6703.

51. Haris, P. I.; Robillard, G. T.; van Dijk, A. A.; Chapman, D., Potential of carbon-13 and nitrogen-15 labeling for studying protein-protein interactions using Fourier-transform infrared spectroscopy. *Biochemistry* **1992,** 31, 6279-6284.

52. Tadesse, L.; Nazarbaghi, R.; Walters, L., Isotopically enhanced infrared spectroscopy: A novel method for examining secondary structure at specific sites in conformationally heterogeneous peptides. *J. Am. Chem. Soc.* **1991,** 113, 7036-7037.

53. Zhang, M.; Fabian, H.; Mantsch, H. H.; Vogel, H. J., Isotope-edited Fourier transform infrared spectroscopy studies of Calmodulin's interaction with its target peptides. *Biochemistry* **1994,** 33, 10883-10888.

54. Barber-Armstrong, W.; Donaldson, T.; Wijesooriya, H.; Gangani, R. A.; Silva, D.; Decatur, S. M., Empirical relationships between isotope-edited IR spectra and helix geometry in model peptides. *J. Am. Chem. Soc.* **2004,** 126, 2339−2345.

55. Decatur, S. M., Elucidation of residue-level structure and dynamics of polypeptides via isotopp-edited infrared spectroscopy. *Acc. Chem. Res.* **2006,** 39, 169−175.

56. Decatur, S. M.; Antonic, J., Isotope-edited infrared spectroscopy of helical peptides. *J. Am. Chem. Soc.* **1999,** 121, 11914−11915.

57. Petty, S. A.; Decatur, S. M., Experimental evidence for the reorganization of β-strands within aggregates of the Aβ(16−22) peptide. *J. Am. Chem. Soc.* **2005,** 127, 13488−13489.

58. Huang, R.; Kubelka, J.; Barber-Armstrong, W.; Silva, R. A. G. D.; Decatur, S. M.; Keiderling, T. A., Nature of vibrational coupling in helical peptides: An isotopic labeling study. *J. Am. Chem. Soc.* **2004,** 126, 2346-2354.

59. http://en.wikipedia.org/wiki/Heavy_water.

60. Fisher, S. J.; Helliwell, J. R., An investigation into structural changes due to deuteration. *ACTA Crystallogr. A* **2008,** 64, 359−367.

61. Kushner, D. J.; Baker, A.; Dunstall, T. G., Pharmacological uses and perspectives of heavy water and deuterated compounds. *Can. J. Physiol. Pharmacol.* **1999,** 77, 79−88.

62. Efimova, Y. M.; Haemers, S.; Wierczinski, B.; Norde, W.; van Well, A. A., Stability of globular proteins in H_2O and D_2O. *Biopolymers* **2007,** 85, 264−273.

63. http://webbook.nist.gov/cgi/cbook.cgi?ID=C7732185&Units=SI&Type=IR-SPEC&Index=1#IR-SPEC.

64. Valenti, L. E.; Paci, M. B.; De Pauli, C. P.; Giacomelli, C. E., Infrared study of trifluoroacetic acid unpurified synthetic peptides in aqueous solution: Trifluoroacetic acid removal and band assignment. *Anal. Biochem.* **2009,** 410, 118-123.

65. Hassler, N.; Baurecht, D.; Reiter, G.; Fringeli, U. P., In Situ FTIR ATR spectroscopic study of the interaction of immobilized human serum albumin with cholate in aqueous environme. *J. Phys. Chem. C* **2011,** 115, 1064-1072.

66. Cai, P.; Flach, C. R.; Mendelsohn, R., An infrared reflection-absorption spectroscopy study of the secondary structure in (KL4)(4)K, a therapeutic agent for respiratory distress syndrome, in aqueous monolayers with phospholipids. *Biochemistry* **2003,** 42, 9446-9452.

67. Ramajo, A. P.; Petty, S. A.; Starzyk, A.; Decatur, S. M.; Volk, M., The α-helix folds more rapidly at the C-terminus than at the N-terminus. *J. Am. Chem. Soc.* **2005,** 127, 13784-13785

68. Petty, S. A.; Decatur, S. M., Intersheet rearrangement of polypeptides during nucleation of β-sheet aggregates. *Proc. Nat. Acad. Sci. U.S.A.* **2005,** 102, 14272-14277

69. Starzyk, A.; Barber-Armstrong, W.; Sridharan, M.; Decatur, S. M., Spectroscopic evidence for backbone desolvation of helical peptides by 2,2,2-trifluoroethanol: An isotope-edited FTIR study. *Biochemistry* **2005,** 44, 369-376.

70. Max, J.; Chapados, C., Infrared titration of NaOH by aqueous HCl. *Can. J. Chem.* **2000,** 78, 64-72.

71. Fields, G. B., *Methods in Enzymology*. Academic Press Inc.: New Yorker, 1997; Vol. 289.

72. Kates, S. A.; Albericio, F., *Solid-Phase Synthesis, a Practical Guide*. Marcel Dekker, Inc.: New York, 2000.

73. Fields, G. B.; Noble, R. L., Solid-phase peptide synthesis utilizing 9-flourenylmethoxycarbonyl amino acids. *Int. J. Pept. Prot. Res.* **1990,** 35, 161-214.

74. Shanmugam, G.; Polavarapu, P. L., Site-specific structure of Aβ(25-35) peptide: Isotope-assisted vibrational circular dichroism study. *Biochim. Biophys. Acta* **2013,** 1834, 308-316.

75. Sanchez-Gonzalez, I.; Carmona, P.; Moreno, P.; Borderias, J.; Sanchez-Alonso, I.; Rodriguez-Casado, A.; Careche, M., Protein and water structural changes in fish surimi during gelation as revealed by isotopic H/D exchange and Raman spectroscopy. *Food Chem.* **2008,** 106, 56-64.

76. Gaggelli, E.; Kozlowski, H.; Valensin, D.; Valensin, G., Copper homeostasis and neurodegenerative disorders (Alzheimer's, prion, and Parkinson's diseases and amyotrophic lateral sclerosis). *Chem. Rev.* **2006,** 106, 1995−2044.

77. Lemkul, J. A.; Bevan, D. R., Destabilizing Alzheimer's Aβ42 protofibrils with morin: mechanistic insights from molecular dynamics simulations. *Biochemistry* **2010,** 49, 3935−3946.

78. Lowe, T. L.; Strzelec, A.; Kiessling, L. L.; Murphy, R. M., Structure-Function relationships for inhibitors of β-amyloid toxicity containing the recognition sequence KLVFF. *Biochemistry* **2001,** 40, 7882−7889.

79. Scheidt, H. A.; Morgado, I.; Rothemund, S.; Huster, D., Dynamics of amyloid-β fibrils revealed by solid-state NMR. *J. Biol. Chem.* **2012,** 287, 2017-2021.

80. Petkova, A. T.; Ishii, Y.; Balbach, J. J.; Antzutkin, O. N.; Leapman, R. D.; Delaglio, F.; Tycko, R., A structural model for Alzheimer's β-amyloid fibrils based on experimental constraints from solid state NMR. *Proc. Natl. Acad. Sci. U. S. A.* **2002,** 99, 16742−16747.

81. Cole, N. B.; Murphy, D. D.; Lebowitz, J.; Di Noto, L.; Levine, R. L.; Nussbaum, R. L., Metal-catalyzed oxidation of α-synuclein - Helping to define the relationship between oligomers, protofibrils, and filaments. *J. Biol. Chem.* **2005,** 280, 9678−9690.

82. Danzer, K. M.; Haasen, D.; Karow, A. R.; Moussaud, S.; Habeck, M.; Giese, A.; Kretzschmar, H.; Hengerer, B.; Kostka, M., Different species of α-synuclein oligomers induce calcium influx and seeding. *J. Neurosci.* **2007,** 27, 9220−9232.

83. Dusa, A.; Kaylor, J.; Edridge, S.; Bodner, N.; Hong, D.; Fink, A. L., Characterization of oligomers during α-synuclein aggregation using intrinsic tryptophan fluorescence. *Biochemistry* **2006,** 45, 2752−2760.

84. Goers, J.; Uversky, V. N.; Fink, A. L., Polycation-induced oligomerization and accelerated fibrillation of human α-synuclein in vitro. *Protein Sci.* **2003,** 12, 702−707.

85. Kostka, M.; Hogen, T.; Danzer, K. M.; Levin, J.; Habeck, M.; Wirth, A.; Wagner, R.; Glabe, C. G.; Finger, S.; Heinzelmann, U.; Garidel, P.; Duan, W.; Ross, C. A.; Kretzschmar, H.; Giese, A., Single particle characterization of iron-

induced pore-forming α-synuclein oligomers. *J. Biol. Chem.* **2008,** 283, 10992–11003.

86. Lowe, R.; Pountney, D. L.; Jensen, P. H.; Gai, W.; Voelcker, N. H., Calcium(II) selectively induces α-synuclein annular oligomers via interaction with the C-terminal domain. *Protein Sci.* **2004,** 13, 3245–3252.

87. van Rooijen, B. D.; Claessens, M. M. A. E.; Subramaniam, V., Membrane binding of oligomeric α-synuclein depends on bilayer charge and packing. *FEBS Lett.* **2008,** 582, 3788–3792.

88. Yamin, G.; Uversky, V. N.; Fink, A. L., Nitration inhibits fibrillation of human α-synuclein in vitro by formation of soluble oligomers. *FEBS Lett.* **2003,** 542, 147–152.

89. Zhu, M.; Han, S.; Zhou, F.; Carter, S. A.; Fink, A. L., Annular oligomeric amyloid intermediates observed by in situ atomic force microscopy. *J. Biol. Chem.* **2004,** 279, 24452–24459.

90. Gangani, R. A.; Silva, D.; Barber-Armstrong, W.; Decatur, S. M., The organization and assembly of a β-sheet formed by a prion peptide in solution: An isotope-edited FTIR study. *J. Am. Chem. Soc.* **2003,** 125, 13674-13675.

91. Petty, S. A.; Adalsteinsson, T.; Decatur, S. M., Correlations among morphology, β-sheet stability, and molecular structure in prion peptide aggregates. *Biochemistry* **2005,** 44, 4720-4726.

92. Thirumalai, D.; Reddy, G.; Straub, J. E., Role of water in protein aggregation and amyloid polymorphism. *Acc. Chem. Res.* **2012,** 45, 83-92.

93. Bernstein, S. L.; Dupuis, N. F.; Lazo, N. D.; Wyttenbach, T.; Condron, M. M.; Bitan, G.; Teplow, D. B.; Shea, J. E.; Ruotolo, B. T.; Robinson, C. V.; Bowers, M. T., Amyloid-beta protein oligomerization and the importance of tetramers and dodecamers in the aetiology of Alzheimer's disease. *Nature Chem.* **2009,** 1, 326-331.

94. Ono, K.; Condron, M. M.; Teplow, D. B., Structure-neurotoxicity relationships of amyloid-β protein oligomers. *Proc. Nat. Acad. Sci. U.S.A.* **2009,** 106, 14745-14750.